A Systematic Comparison of Tropical Waves over Northern Africa. Part I: Influence on Rainfall

ANDREAS SCHLUETER, ANDREAS H. FINK, AND PETER KNIPPERTZ

Institute of Meteorology and Climate Research, Karlsruhe Institute of Technology, Karlsruhe, Germany

PETER VOGEL

Institute of Meteorology and Climate Research, and Institute for Stochastics, Karlsruhe Institute of Technology, Karlsruhe, Germany

(Manuscript received 23 March 2018, in final form 21 November 2018)

ABSTRACT

Low-latitude rainfall variability on the daily to intraseasonal time scale is often related to tropical waves, including convectively coupled equatorial waves, the Madden–Julian oscillation (MJO), and tropical disturbances (TDs). Despite the importance of rainfall variability for vulnerable societies in tropical Africa, the relative influence of tropical waves for this region is largely unknown. This article presents the first systematic comparison of the impact of six wave types on precipitation over northern tropical Africa during the transition and full monsoon seasons, using two satellite products and a dense rain gauge network. Composites of rainfall anomalies in the different datasets show comparable modulation intensities in the West Sahel and at the Guinea Coast, varying from less than 2 to above 7 mm day^{-1} depending on the wave type. African easterly waves (AEWs) and Kelvin waves dominate the 3-hourly to daily time scale and explain 10%–30% locally. On longer time scales (7–20 days), only the MJO and equatorial Rossby (ER) waves remain as modulating factors and explain about up to one-third of rainfall variability. Eastward inertio-gravity waves and mixed Rossby–gravity (MRG) waves are comparatively unimportant. An analysis of wave superposition shows that low-frequency waves (MJO, ER) in their wet phase amplify the activity of high-frequency waves (TD, MRG) and suppress them in the dry phase. The results stress that more attention should be paid to tropical waves when forecasting rainfall over northern tropical Africa.

1. Introduction

Rainfall variability substantially affects societies in northern tropical Africa (Sultan et al. 2005). More than 96% of cultivated land in sub-Saharan Africa is rain-fed (FAO 2016). Despite this, major operational global weather prediction models still fail to deliver skillful short-range precipitation forecasts over this region (Vogel et al. 2018). This corroborates the need for an improved understanding of the underlying processes involved in the generation of precipitation and their representation in numerical weather prediction (NWP) models over northern tropical Africa.

Equatorial waves are a potential source of predictability in the tropics, as they can be considered preferred eigenmodes of the tropical atmosphere. These waves can couple with deep convection and subsequently modulate rainfall on the synoptic to subseasonal time scale throughout the tropics (Wheeler and Kiladis 1999). Equatorial waves interacting with precipitation are thus called convectively coupled equatorial waves (CCEWs). Several different types of CCEWs have been identified, which differ in their wavelength and period as well as in their accompanying influence on the dynamic and thermodynamic environment. The solutions of the shallow-water equations, a theory describing wave propagation trapped at the equator, include the equatorial Rossby (ER) wave, the mixed Rossby–gravity

Denotes content that is immediately available upon publication as open access.

Supplemental information related to this paper is available at the Journals Online website: https://doi.org/10.1175/JCLI-D-18-0173.s1.

Corresponding author: Andreas Schlueter, andreas.schlueter@kit.edu

DOI: 10.1175/JCLI-D-18-0173.1

(MRG) wave, the Kelvin wave, and eastward and westward propagating inertio-gravity (EIG and WIG) waves (Matsuno 1966). Two other major wave types have been observed in the tropical belt that are not obtained from the shallow-water equations: the Madden–Julian oscillation (MJO; Madden and Julian 1971) and westward traveling tropical disturbances (TDs) including easterly waves (Riehl 1945). All these waves are collectively termed "tropical waves" in this paper. The spatiotemporal scales range from planetary and 30–90 days in the case of the MJO to synoptic and 1–3 days in the case of inertio-gravity waves.

Rainfall over northern tropical Africa exhibits substantial variability at the synoptic to intraseasonal time scales. Three different regimes have been identified: the synoptic time scale, with oscillatory signals of periods below 10 days; the short intraseasonal time scale with periods from 10 to 25 days; and the long intraseasonal time scale, with periods from 25 to 60 days (Janicot et al. 2011). On the short intraseasonal time scale, two main modes have been documented: the "quasi-biweekly zonal dipole" (QBZD; Mounier et al. 2008) and the "Sahel" mode (Sultan and Janicot 2003). Besides radiative processes, the QBZD has been associated with the presence of Kelvin waves, whereas ER waves appear to contribute to the Sahel mode (Janicot et al. 2010). Finally, the variability of the Saharan heat low also modulates rainfall at the time scale of 10–25 days (Chauvin et al. 2010; Roehrig et al. 2011).

The dominant influence of African easterly waves (AEWs) on precipitation over West Africa has been known for several decades (Reed et al. 1977). AEWs modulate precipitation on the time scale of 2–6 days. About one-third of the total variance in deep convection can be explained by 2–6-day filtered disturbances (Dickinson and Molinari 2000; Mekonnen et al. 2006; Lavaysse et al. 2006; Skinner and Diffenbaugh 2013). According to Fink and Reiner (2003), more than 60% of squall lines in West Africa, which are responsible for the vast majority of rainfall in this region, are associated with AEWs. Roundy and Frank (2004) show that TDs, which are observed in the entire tropics, correspond to AEWs over northern tropical Africa. Following Roundy and Frank (2004), the term TD will refer to AEWs throughout this paper.

Kelvin waves modulate rainfall on the synoptic to intraseasonal time scale. During the boreal spring, rainfall over central Africa is significantly influenced by Kelvin waves (Nguyen and Duvel 2008; Laing et al. 2011; Sinclaire et al. 2015). Mekonnen et al. (2008) demonstrate that Kelvin waves double the observed rainfall amount over tropical Africa during the full monsoon. Over West Africa, Kelvin waves explain 10%–15% of convective variability (Mekonnen and Thorncroft 2016). Kelvin waves are not isolated features; instead, they also interact with AEWs or trigger them (Mekonnen et al. 2008; Ventrice and Thorncroft 2013; Mekonnen and Thorncroft 2016).

On the intraseasonal time scale, the influence of the MJO on precipitation over northern tropical Africa has been discussed by several authors (e.g., Matthews 2004; Janicot et al. 2009; Lavender and Matthews 2009; Ventrice et al. 2011; Alaka and Maloney 2017). The MJO significantly modulates the dry spell frequency in the West Sahel as station data suggest (Pohl et al. 2009). Gu (2009) and Pohl et al. (2009) document a more pronounced modulation of precipitation along the Guinean belt. During the spring season, the MJO was found to modulate precipitation in central Africa (Berhane et al. 2015).

ER waves mainly modulate precipitation on the subseasonal time scale. In a detailed study of ER waves over West Africa, Janicot et al. (2010) distinguish two different types of ER waves. The imprint of the first mode on the 30–100-day time scale is linked to the MJO and modulates convection over central and West Africa. On the time scale of 10–30 days, ER waves also modulate precipitation in the Sahelian band. The influence of the slightly tilted poleward and eastward second mode can be seen reaching far into the subtropics and suggests a link to extratropical circulation. The slightly eastward tilted precipitation pattern resemble tropical plumes regularly observed during the dry winter season (Knippertz and Martin 2005; Fröhlich et al. 2013).

In the literature, little attention has been paid to MRG waves over this region. Results by Skinner and Diffenbaugh (2013) indicate that MRG contribute less to rainfall variability than TD, Kelvin, and ER waves. They are most frequently observed in the central and western Pacific region, where they significantly affect precipitation (Takayabu and Nitta 1993; Holder et al. 2008; Kiladis et al. 2016). MRG waves occur in a wave domain next to TD. Over the Pacific Ocean, the transition of MRG to off-equatorial TDs has been documented (Takayabu and Nitta 1993; Zhou and Wang 2007). Similarly, "hybrid" AEW/MRG waves have been documented over Africa (Y.-M. Cheng et al. 2018, personal communication). However, the involved mechanisms are still not fully understood. More research is needed to clarify how MRG waves and AEWs interact and to integrate disturbances that do not follow either of their characteristics, as mentioned by Knippertz et al. (2017).

Only a few studies have focused on EIG and WIG waves so far. Dry EIG waves in the mesosphere and stratosphere have been recorded by Mayr et al. (2003, 2004), Tindall et al. (2006a), and Tindall et al. (2006b).

Some evidence suggests that EIG can be also found in the troposphere with main influence on upper levels (Yang et al. 2003, 2007; Kiladis et al. 2009), although they are not completely separable from MRG waves (Kiladis et al. 2016; Dias and Kiladis 2016). WIG waves were identified as associated with squall lines, which are the main cause for precipitation in the Sahel region (Tulich and Kiladis 2012). Whether EIG and WIG waves also influence rainfall variability over northern tropical Africa is largely unknown.

Despite the importance of the different types of tropical waves on the variability of rainfall on synoptic to intraseasonal time scales over northern tropical Africa, as of today a systematic investigation of the relative influence of the different waves on rainfall variability has not been performed. Several questions concerning the modulation of rainfall by the different waves remain open. The quantitative influence of tropical waves and the relative contribution to rainfall variability at the different time scales are not well documented and a consistent analysis for all waves using a unified method is pending. Operational forecasters in the region mostly rely on their experience or subjective view when assessing tropical waves because little is known about the relative influence of the different waves at the different time scales, as it has not yet been quantified systematically (B. Lamptey 2017, personal communication). The aim of the present study is therefore to close this gap and compare the influence of the major types of tropical waves for the monsoon system of Africa using satellite products and in situ measurements, and one consistent method for all waves. The forecast verification study of Vogel et al. (2018) has stressed the need to use data from rain gauge networks due to large discrepancies between satellite and rain gauge accumulations in this region at daily time scales. Thus, the present study also uses an extensive database of African rain gauges.

This article will present a comparative study of the influence of tropical waves on precipitation over northern tropical Africa. As the region receives its main rainfall during the ''full monsoon'' and the months before and after the onset in the so-called ''transition season'', this paper will focus on these two seasons. This study follows in parts the work of van der Linden et al. (2016), who performed a similar systematic study on the modulation of precipitation by three tropical waves over Vietnam. The following research questions will be addressed:

- Where, in which season, and how strongly do tropical waves contribute to rainfall variability over northern tropical Africa?
- What is their effect on spatial precipitation patterns and observed rainfall amounts?
- What is their relative contribution to rainfall variability on different time scales?
- Do different types of tropical waves interact when they superimpose?

After the description of the used data and filtering methods in section 2, answers to these four questions are presented and discussed in section 3. Section 4 concludes this study. A companion study will put the results of this paper into context with the influence the waves exert on dynamic and thermodynamic conditions of the West African monsoon.

2. Methods

a. Study area

This study focuses on two 5°-wide latitudinal bands in northern tropical Africa (Fig. 1): the Guinean (5°–10°N) and Sahelian band (10°–15°N). For a more detailed analysis, two boxes in West Africa were defined where most rain gauges are available: the Guinea Coast (5°W–5°E, 5°–10°N) and the West Sahel (5°W–5°E, 10°–15°N). The analysis was stratified in two seasons: the ''full monsoon'' ranges from July to September; the three months before the onset of the monsoon (from April to June) and October are collectively labeled as the ''transition season'' (Sultan et al. 2003; Thorncroft et al. 2011); combining both, the ''extended monsoon season'' stretches from April to October.

b. Data

The modulating impact of tropical waves on rainfall over northern tropical Africa was examined in three different rainfall datasets. The Tropical Rainfall Measuring Mission (TRMM) 3B42 V.7 precipitation dataset is arguably the most accurate gridded rainfall product for the tropics (Maggioni et al. 2016), with a record long enough for climatological studies. TRMM 3B42 is a gauge-adjusted combined microwave–IR precipitation estimate (Huffman et al. 2007). It has been used in several studies of tropical waves (e.g., Yasunaga and Mapes 2012; Lubis and Jacobi 2015). The 3-hourly product has a spatial resolution of 0.25° × 0.25°. The analyzed time period ranges from 1998 to 2016. With full spatial coverage in the tropics and a high temporal and spatial resolution, the TRMM dataset is a preferable dataset for the study of tropical waves in a rain gauge sparse environment such as tropical Africa.

For a 33-yr period from 1981 to 2013, the Climate Hazards Group Infrared Precipitation with Station Data V.2 (CHIRPS) provides daily, gauge-calibrated,

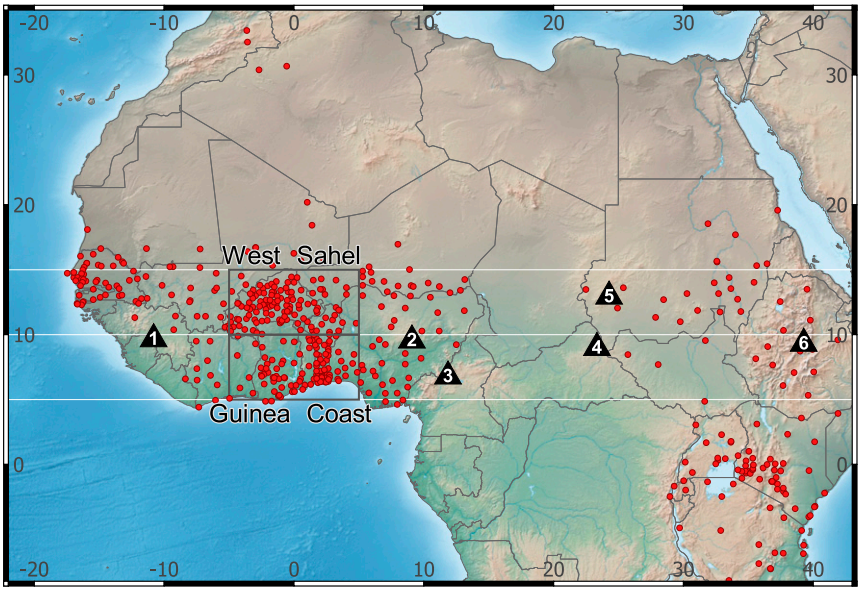

FIG. 1. Topographic map of the study area. Available stations with a minimum of 50% observations during 1981–2013 are indicated by a red dot. The two boxes show the location of the Guinea Coast and West Sahel used in this study. Black triangles show prominent orographic features that are discussed in the text: 1) Guinea Highlands, 2) Jos Plateau, 3) Cameroon Line, 4) Bongo Massif, 5) Darfur Mountains, and 6) Ethiopian Highlands.

infrared-based precipitation estimates (Funk et al. 2015). The dataset has a resolution of 0.25° × 0.25° and is available over landmasses only. The daily CHIRPS product that was used is disaggregated from 5-day accumulated values. Because of the disaggregation, CHIRPS can only be used with care at daily time scales and will likely underestimate the variability when compared to rain gauge observations (C. Funk 2017, personal communication). At 0°E, the daily values range from 0000 to 0000 UTC + 1 day. This dataset has the advantage of a long record and a high spatial resolution. On the other hand, it has a comparatively low temporal resolution and is only available over the continent.

In situ rain gauge measurements are essential to validate the results obtained from satellite observations. The Karlsruhe African Surface Station Database (KASS-D) provides daily measurements from an extended rain gauge network. The 24-h accumulation period ranges for most stations from 0600 to 0600 UTC. Stations were required to have at least 50% of observations during the period from 1981 to 2013 to match with the analyzed time period of the CHIRPS dataset. Additionally, stations with less than 1% of nonzero observations were excluded, resulting in a total number of 524 stations (Fig. 1).

A good proxy for tropical convection is outgoing longwave radiation [OLR; see review in Arkin and Ardanuy (1989)]. OLR has been successfully applied in other studies of tropical waves (e.g., Wheeler and Kiladis 1999; Roundy and Janiga 2012). Therefore, the daily interpolated National Oceanic and Atmospheric Administration (NOAA) OLR dataset (Liebmann and Smith 1996) was used to filter the waves in the period from 1981 to 2013. The spatial resolution of this dataset is 2.5° × 2.5°. To demonstrate the effect of orography, we used the 5-min gridded ETOPO5 elevation dataset (NGDC 1988).

c. *Wave filtering*

Six different wave types were analyzed in this study, sorted according to their scale: MJO, ER, MRG, Kelvin, TD, and EIG ($n = 0$, hereafter simply called EIG) waves. WIG and higher meridional mode EIG ($n > 1$) could not be analyzed because their frequency is too high to be filtered in daily data. The activities of the tropical waves were filtered in the wavenumber–frequency spectrum following the method developed by Wheeler and Kiladis (1999). The filter settings for wavenumber, frequency, and equivalent depth ranges are obtained from previous studies on tropical waves studies (Table 1). No symmetric/antisymmetric decomposition has been done as the analyzed bands are entirely north of the equator. A small overlap of the filter bands of Kelvin and EIG waves, and of TD and MRG waves exists, which is likely not important. It has to be noted that the wave signal, as captured by the filter bands, can be contaminated by random noise. The

TABLE 1. Analyzed tropical waves with their corresponding wave characteristics. The filter settings for the period ω, the wavenumber k, and the shallow water depth h were used to extract the wave signal. Corresponding references are given.

Acronym	Wave	Direction	ω (days)	k	h (m)	Source
MJO	Madden–Julian oscillation	Eastward	30–96	0–9	—	Roundy and Frank (2004)
ER	Equatorial Rossby wave	Westward	9–72	1–10	1–90	Kiladis et al. (2009)
MRG	Mixed Rossby–gravity wave	Westward	3–8	1–10	8–90	Wheeler and Kiladis (1999)
Kelvin	Kelvin wave	Eastward	2.5–20	1–14	8–90	Wheeler and Kiladis (1999)
TD/AEW	Tropical disturbance/African easterly wave	Westward	2.5–5	6–20	—	Lubis and Jacobi (2015)
EIG	Eastward inertio-gravity wave	Eastward	1–5	0–14	12–50	Yasunaga and Mapes (2012)

obtained signal must be interpreted as an overestimate of the wave modulation since wave motions generally stay out against the background noise by less than 30% (Wheeler and Kiladis 1999).

The modulation of precipitation by tropical waves was investigated for two periods: 1) for the shorter period from 1998 to 2016, the influence of tropical waves was analyzed in the TRMM dataset, and 2) for the longer period from 1981 to 2013, CHIRPS and KASS-D were examined. Table 2 shows the structure of the results section and lays out which dataset has been used in which subsection. For the analysis of the rainfall patterns and modulation intensities of each wave, OLR is used by default for the wave filtering to derive the local wave phase. Precipitation anomalies or quantile deviations are then projected onto this composite. TRMM data have also been used in place of OLR to determine the wave phase (see the online supplemental material) to assess the robustness of the composite. For the analysis of the contribution of each wave to the rainfall variability and the wave interaction, TRMM has been wave-filtered directly because of its global coverage, which is required for the wave filtering.

The filtering was done using the NCAR Command Language (NCL) ''kf_filter'' function. This function is based on a fast Fourier transform (FFT), which does not allow missing values in the entire analyzed latitudinal band. For the longer period from 1981 to 2013, we rely on the interpolated OLR dataset as a proxy for precipitation, although the relationship between OLR and precipitation is weak over West Africa (see Fig. S1 in the online supplemental material). CHIRPS is available only over the continents and could thus not be used for filtering. The 3-hourly TRMM product exhibits minor observational gaps. Over Africa, these gaps are negligible with an average amount of missing data of about 0.005% to 0.05%. All missing values in TRMM were filled with zeros. The effect of this primitive gap filling method for the wave filtering is expected to be negligible over Africa where gaps are rare. As a side remark, more caution should be applied when the 3-hourly TRMM product is used for wave filtering over the Maritime Continent for the period prior to 2007, where about 1% of the data is missing due to downtimes of a geostationary IR satellite.

The filtering method has no constraints for the associated circulation. Wave signals can be contaminated by physically different phenomena, missed by the filter due to Doppler shifting, or double counted due to the partial overlap of wavenumber frequency spectra. Other filters have been developed that are based on the horizontal structure functions obtained from equatorial

TABLE 2. Structure of the study and use of datasets. The table lists the subsections in the results part and outlines which datasets have been used to filter for the tropical waves and which precipitation datasets have been subsequently plotted in the corresponding figures.

Section	Topic	Wave filtered dataset	Plotted dataset (raw, composite, correlation)	Figures
3a	Mean climate	—	TRMM	Fig. 3
3b	Total variance of wave activity	TRMM	TRMM	Fig. 4
3c	Modulation patterns	OLR	CHIRPS, KASSD	Figs. 5–6
3d	Modulation intensity	OLR	CHIRPS	Fig. 7
		OLR	KASSD	Figs. 7–8
		TRMM	TRMM	Fig. 7
3e	Relative contribution to precipitation	TRMM	TRMM	Figs. 9–11
3f	The role of orography	TRMM	TRMM	Figs. 9–11
3g	Wave interactions	TRMM	TRMM	Fig. 12

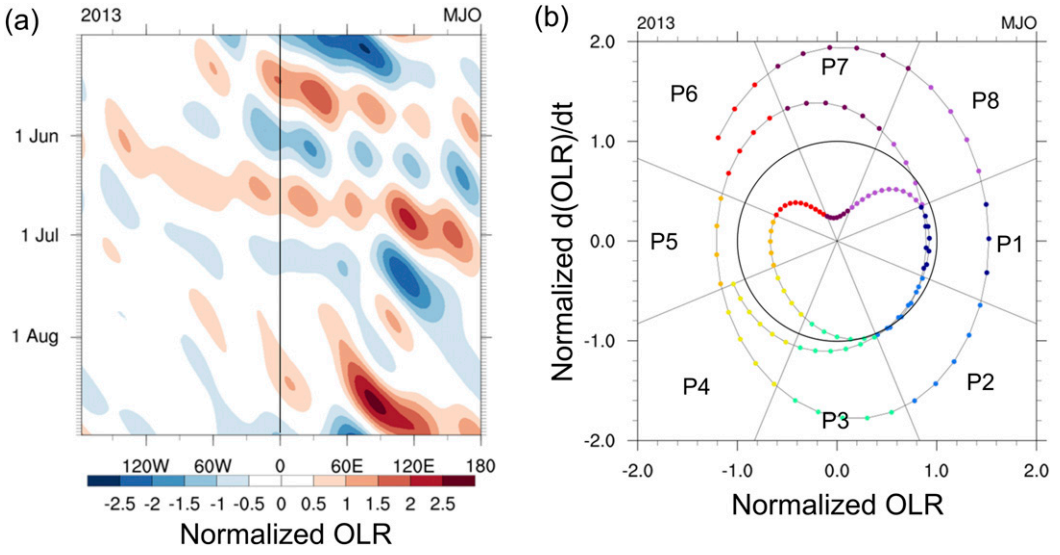

FIG. 2. Construction of composite plots. (a) Example of a Hovmöller diagram of an MJO filtered normalized OLR signal. Negative anomalies correspond to wet conditions. (b) Example for the MJO in a phase diagram. Plotting the wave filtered signal at 0°E [black line in (a)] against the time derivative at 0°E results in a phase diagram of the local wave activity. The phase space is divided into eight phases (coloring); dates when the amplitude is less than one standard deviation are considered to be inactive.

wave theory (Yang et al. 2003), use wavelent analysis (e.g., Kikuchi and Wang 2010; Roundy 2018), or 3D normal mode functions (Castanheira and Marques 2015). Nonetheless, the method applied here has been successfully used in previous studies over Africa (e.g., Mounier et al. 2007, 2008; Janicot et al. 2009, 2010; Ventrice and Thorncroft 2013; Mekonnen and Thorncroft 2016). In a subsequent article it will be shown that composites of dynamical fields using this method are able to reproduce the circulation patterns that are expected from wave theory.

As a metric for the MJO activity, several EOF-based global indices have been proposed, such as the Real-Time Multivariate MJO (RMM; Wheeler and Hendon 2004) index and the OLR-based MJO Index (OMI; Kiladis et al. 2014). These indices have the advantage of measuring the global propagation of the MJO and being less affected by background noise. Over Africa, conversely, the MJO manifests itself rather as a standing signal (Alaka and Maloney 2012, 2014, 2017). A local wave filtering, as applied in this study, will thus mainly depict the standing signal over Africa and might miss the global propagative signal as seen over the Indian and Pacific Oceans.

d. Composite analysis

Composites of the waves were constructed to investigate the propagation and structure of modulation patterns by averaging rainfall anomalies over all dates during the extended monsoon season when the wave is in a specific phase based on the OLR signal (see Figs. 5 and 6). A local wave phase and amplitude is defined following the method initially developed by Riley et al. (2011) for the MJO. The filtered wave signal and its corresponding time derivative are calculated for a reference location in West Africa at 0°E and 5°–15°N (Fig. 2a). Both fields are standardized by dividing by the standard deviation of the respective field. The phase diagram is then split in eight equal phases (Fig. 2b). Phase 1 refers to a local dry phase over the reference location, and phase 5 to the wet phase; during phases 3 and 7 the wave is in its neutral phase, and the rest of the phases are transition phases. During dates when the amplitude of the wave activity is less than one standard deviation, the wave is considered to be inactive. For a more detailed description of the calculation of wave phases, the reader is referred to Yasunaga and Mapes (2012) and van der Linden et al. (2016), where this approach is also applied to study the local influence of tropical waves. For all waves about 400–450 days are available in each phase. Additional maps showing the anomalies based on TRMM filtered waves instead of OLR are available in the supplemental material (Figs. S7–S12). These maps are not as smooth as the plots obtained from CHIRPS, because the sample size is smaller due to the shorter period from 1998 to 2013; they have, however, the advantages that the wave signal is directly filtered from precipitation instead of OLR and

that they include rainfall anomalies over the ocean. As a side remark, it was tested whether OLR-filtered TRMM composites are less noisy. However, the noisiness was not removed and the general patterns did not change significantly (not shown). Statistical significance of the anomalies in the composite analysis (Figs. 5 and 6) is calculated using nonparametric bootstrapping. Significance was tested at a 5% level using a sample of 1000 repetitions. The compositing method mostly removes the background noise, and the resultant patterns reflect at least to first order the linear relationship to the analyzed wave.

e. Normalization of precipitation

The composite maps of rainfall require a prior normalization. Northern tropical and subtropical Africa features a wide range of different climates. Annual precipitation ranges from more than 2500 mm yr^{-1} in coastal perhumid areas of western and central Africa to less than 100 mm yr^{-1} in the hyperarid areas in the Saharan Desert (Fink et al. 2017). To make the effect of tropical waves on precipitation anomaly patterns comparable for these very diverse climates, precipitation values need to be normalized. Using total rainfall anomalies, the modulation in drier regions would not be visible. Indices like the standardized precipitation index (SPI) (McKee et al. 1993) cannot be calculated on the daily time scale. Here, we propose to use a quantile-based approach instead, in order to derive normalized daily precipitation anomalies against a climatological reference. An adjusted definition of quantiles was used to account correctly for identical values and, in particular, the many zero observations in hyperarid regions. We define the quantile q for an observation y and set of climatological observations O of size N as

$$q(y) := \frac{|\{a \in O | a < y\}| + \frac{1}{2}|\{b \in O | b = y\}|}{N}.$$

In other words, q gives the percentage of observations a that are smaller than y plus half the percentage of observations b that are equal to y, both relative to the total number of observations. The later part is done to equally weigh observations with the same value. By definition, the median of the climatology equals to $\tilde{q} = 50\%$. Anomalies are then calculated as deviations from the median, resulting in quantile anomalies as measured in percentiles $a = (100q - 50)\%$. This approach allows us to compare precipitation anomalies of different climates.

To derive a reasonable sample for the reference climatology, the concept of an extended probabilistic climatology is used [see Vogel et al. (2018) for a more detailed discussion]. To increase the sample size and reduce the sampling error, the climatology was defined as a set of observations ±7 days around the respective day of the year. A sample of ±7 days reasonably minimizes the sampling error and bias (Vogel et al. 2018, Fig. S1 in their supplemental material). Larger windows increase the bias due to different climatological settings at the beginning and end of the window.

f. Modulation intensity

Daily rainfall anomalies were computed for the period from 1981 to 2013 for CHIRPS and KASS-D and for the period from 1998 to 2013 for TRMM. Then, the average anomaly during each phase was plotted. For the two focus regions in West Africa, the modulation intensity was measured for all three precipitation datasets. In all, 112 stations are located in the Guinea Coast, whereas the West Sahel box includes 129 stations (Fig. 1). The wave activity in both regions was calculated from OLR for the Guinean (5°–10°N) and Sahelian (10°–15°N) zones, respectively, at 0°E. Most of the stations measure from 0600 to 0600 UTC + 1 day. To remove the time lag of 6 h, we shifted the curve for KASS-D by the estimated length of 6 h measured in wave phases:

$$\Delta P = \frac{6\,\text{h}}{T(\text{in h})/8},$$

where T equals the mean period of the filtered wave signal as determined by the MATLAB function ''meanfreq()''.

The distribution of modulation intensity as seen by different stations was also calculated for both seasons. The mean modulation intensity for each station was calculated by subtracting the mean precipitation in the wettest and driest phase of the eight phases defined above. Because of the potential shift between OLR and the observed station precipitation, the wettest phase is allowed to fall into phases 4–6, whereas the driest phase can lie in phases 8–2.

Kernel density estimation (KDE) has been used to visualize how the modulation intensities vary for the different stations. Commonly, histograms are used to visualize discrete sample of observations. Yet, histograms have disadvantages when visualizing probability density functions (PDFs) of finite samples: They are discontinuous and their shape highly depends on the choice of bin width; additionally, the interpretation of several overlying histograms is rather difficult. A nonparametric alternative to histograms is KDE. To create a smooth and continuous PDF, each observation is weighted with a kernel function. As kernel function

we chose a normal distribution. Results did not differ significantly with a different choice of kernel. The bandwidth h of the kernel was calculated following the rule of thumb by Freedman and Diaconis (1981):

$$h = \frac{2 \times \mathrm{IQR}}{N^{1/3}},$$

where IQR is the interquartile range and N the sample size. An illustrative review explaining KDE and describing the advantages of this method can be found in Gonzales-Fuentes et al. (2015).

g. Correlation analysis

The influence of the different tropical waves is expected to depend on the time scale. For example, daily rainfall variability will be mainly driven by waves with a high frequency such as TD, whereas weekly accumulated rainfall will be mainly determined by low-frequency waves such as the MJO. To test how much of the rainfall variability on different time scales can be explained by the modulation of tropical waves the linear correlation coefficient between the rainfall variability on the specific time scale and the wave filtered signal is calculated. In a first step, the variability on different time scales was calculated, applying a running mean of 1, 3, 7, and 20 days as well as 1° in longitude on the mean TRMM precipitation in the Guinean and Sahelian bands for the transition and full monsoon seasons from 1998 to 2016. This way, the variability on the respective shorter time scales is removed and only the variability on longer time scales is retained. The data are then correlated at each longitude with the wave filtered TRMM signal in the same band. The squared correlation coefficients estimate the explained variance of the rainfall by each wave in this band and during the respective season.

To visualize how the correlation varies within the Guinean and Sahelian bands, the correlations of all waves at each longitude were stacked on top of each other for all time scales (Figs. 9–11). The sum of all correlations should be considered as a maximum percentage that can be explained by tropical waves, as some of the wave bands have small overlaps, and no wave interactions are taken into account. Random noise does not systematically affect the linear correlation, so the correlation shows to first order how much the wave modes contribute to total rainfall variability.

Statistical significance of the correlation coefficients was calculated using a one-sided t test at a significance level of $p < 0.05$. As both time series are autocorrelated in time, the significance test requires a reduced number of degrees of freedom. For two Gaussian distributed, autocorrelated time series x and y of a length N, the reduced degree of freedom ($\mathrm{DF_{eff}}$) is calculated using

$$\mathrm{DF_{eff}} = \frac{N}{1 + 2\sum_{l=0}^{N-1} \frac{N-l}{N} K_x^*(l) K_y^*(l)} + 1,$$

where $K_x^*(l)$ and $K_y^*(l)$ are the autocorrelation functions of both time series [Taubenheim 1974, cited by Fink and Speth (1997)].

h. Wave interactions

The interactions between different types of tropical waves were tested. The mean filtered TRMM precipitation was calculated for the Guinea Coast (5°–10°N, 0°E) and the West Sahel (10°–15°N, 0°E) for the extended monsoon season. Dates when the filtered precipitation exceeded ±1 standard deviation were defined as wet and dry phases of the wave. On average, about 4000 observations fall in each phase for all waves. The average wave-filtered signal in the wet and dry phases is called the primary modulation.

Next, it was analyzed how much a second wave modifies the primary modulation. Therefore, the mean wave-filtered signal of the primary wave was calculated under the condition that a second wave was either in a positive or negative phase. For each possible wave superposition, the sample size was about 500–800 cases. The difference of the mean wave signal during the passage of the second wave to the mean modulation by the primary wave is called the secondary modulation. It should be noted that these values are to be interpreted as the activity in the specific wave spectrum rather than as physical rainfall anomalies. Significant differences were tested using a t test for samples of different variances with a significance level of 5%.

3. Results and discussion

a. Mean climate

The African monsoon system dominates the circulation and distribution of rainfall over northern tropical Africa. During the transition season (April–June; October), when the monsoon has not yet fully started or already ended, rainfall is concentrated over the coastal regions around 5°N (Fig. 3a). Nearly half (49%) of the annual precipitation or a total of ~600 mm falls in the Guinea Coast box during this season as outlined in Fig. 3. In contrast, the West Sahel box receives 28% of the annual precipitation or 230 mm in the same season. With the start of the African monsoon, the main rainfall band moves northward to about 10°N during the full

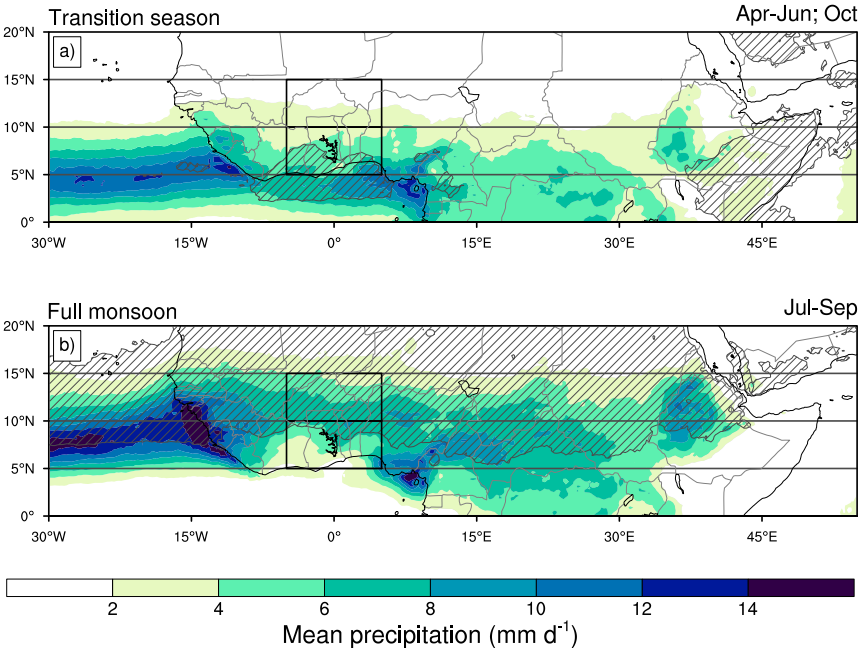

FIG. 3. Mean seasonal precipitation from TRMM observations (1998–2016) during (a) the transition season (April–June; October) and (b) the full monsoon (July–September). Areas with more than 50% of annual rainfall during the respective season are hatched. Black lines denote the boxes and bands as used in subsequent analyses.

monsoon season from July to September (Fig. 3b). Then, 71% of the annual precipitation or 530 mm falls in the West Sahel; the coastal regions of West Africa experience the ''little dry season''. Only 37% of the annual precipitation or 450 mm falls during this season in the Guinea Coast. Because of the West African monsoon, the northward shift is stronger over the land than over the ocean. Rainfall over elevated regions is generally higher than in the lowlands. Prominent orographic features include the Guinea Highlands, the Jos Plateau, the Cameroon Line, the Bongo Massif, the Darfur Mountains, and the Ethiopian Highlands as shown in Fig. 1. It will be demonstrated in section 3e that these orographic features also play a role for how precipitation is modulated by tropical waves.

b. *Total variance of wave activity*

In a first step, it was analyzed where and how much rainfall variability falls into the specific wave spectra during the transition and full monsoon seasons. For this purpose, Fig. 4 shows the standard deviation of wave filtered TRMM precipitation signals during the period from 1998 to 2016. The magnitude of rainfall variability differs in the analyzed wave spectra. CCEW do not show highest variability at the equator as might be expected from the shallow-water equations. Rather, the highest contribution of tropical waves to rainfall variability is directly linked to the mean precipitation patterns and lies where the seasonal rainfall maximum is located. It has to be noted that the background noise significantly contributes to the variance within the different bands and therefore bands with more variance in the raw red spectrum naturally exhibit higher variance in the filtered data as well (cf. Figs. 1 and 2 in Wheeler and Kiladis 1999). The highest variability can be observed for TD and Kelvin waves. During the transition season, TD and Kelvin waves have a comparable variability with a standard deviation of about 3–4 mm day^{-1} at the Guinea Coast. MJO, ER, and MRG are of similar variability with a maximum standard deviation of about 2 mm day^{-1}. The variability in the EIG band is slightly stronger with a maximum standard deviation of about 3 mm day^{-1}.

During the full monsoon in contrast, the TD signal is by far the most dominant source of rainfall variability. The intensity in the TD band increases from the Ethiopian Highlands toward maximum standard deviation of more than 6 mm day^{-1} over the west coast of Africa. The variability for the other waves is comparable with a maximum standard deviation of about 2–3 mm day^{-1}. During this season, ER and MRG waves exhibit slightly more variability, whereas the MJO and Kelvin waves are slightly less active.

Several authors have compared the different waves on a global scale (Wheeler and Kiladis 1999; Roundy

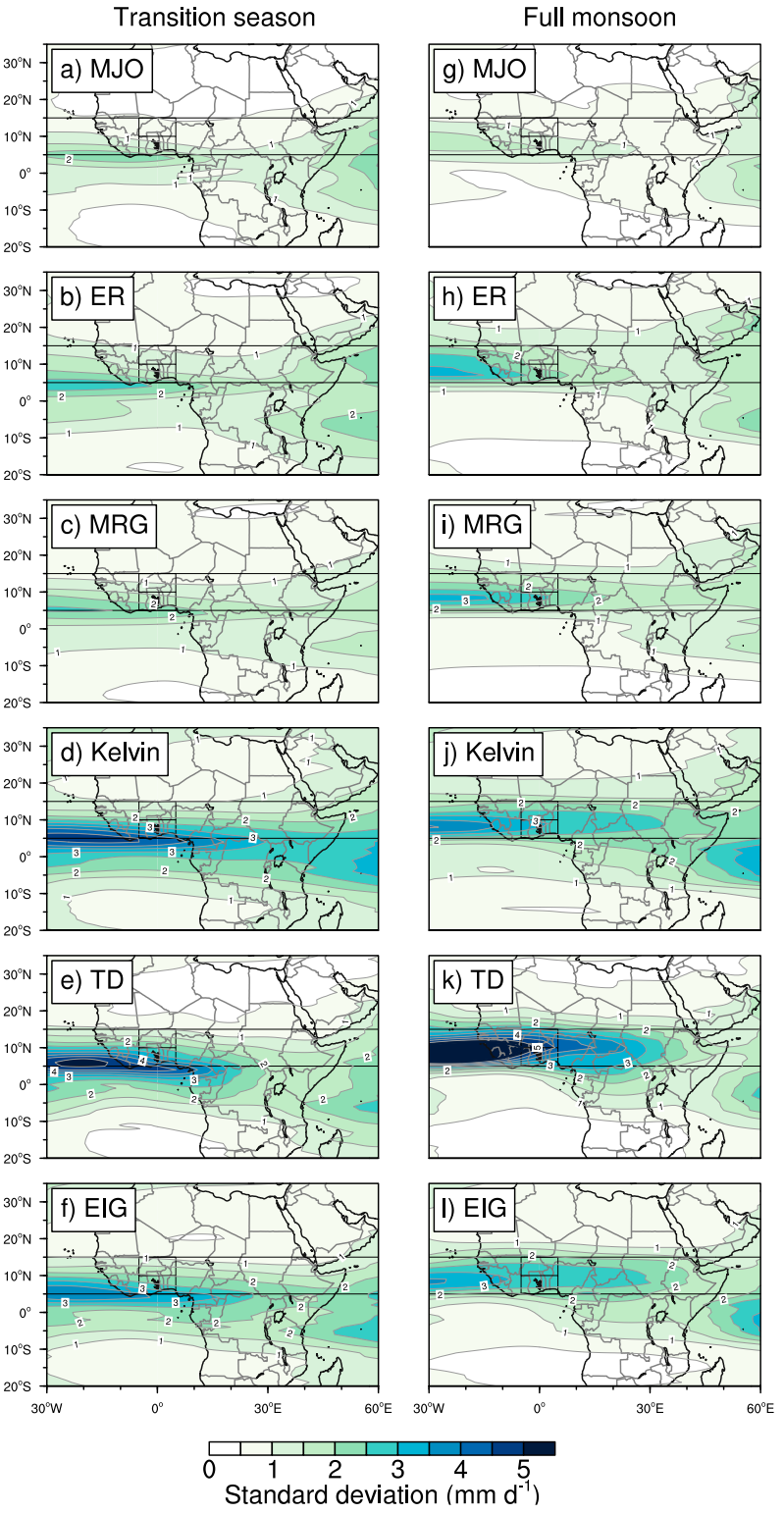

FIG. 4. Standard deviation of TRMM precipitation (1998–2016) within the specific wave domains for (a)–(f) the transition season and (g)–(l) the full monsoon. Black lines denote the boxes and bands as used in subsequent analyses. For abbreviations of wave names, see Table 1.

and Frank 2004; Kiladis et al. 2009; Huang and Huang 2011; Schreck et al. 2013; Lubis and Jacobi 2015). Some of these only provide results for the entire year (Wheeler and Kiladis 1999; Kiladis et al. 2009). The global maps for the summer and spring season in Roundy and Frank (2004) using OLR roughly agree with the results in Fig. 4. The drawback of the studies that filter the waves from OLR or brightness temperature as indicators for deep convection is the low correlation of OLR with daily precipitation over Africa, which is generally less than 0.3 (Fig. S1). Huang and Huang (2011) and Lubis and Jacobi (2015) show the seasonal cycle of different waves demonstrating that the maximum of TD and MRG activity is during the boreal summer, and ER peak during fall and winter, whereas Kelvin waves show the highest activity during boreal spring. Lubis and Jacobi (2015) filter the waves from TRMM precipitation. Their results of the activity of different waves during the extended monsoon season are comparable with the presented results. Skinner and Diffenbaugh (2013) compare in their Fig. 8 the variance of precipitation in different tropical wave spectra over West Africa during June to October in different general circulation models and observations from the Global Precipitation Climatology Project (GPCP). The overall picture is similar: the wave type explaining most variance is TD followed by ER and Kelvin waves. It should be noted that there is considerable inconsistency between the different models and observations, stressing the need for improved representation of the waves in NWP models.

c. *Modulation patterns*

The discussion of Fig. 4 already indicated that different wave types modulate rainfall amounts to a different degree. In a next step, the effect of tropical waves on precipitation patterns and modulation intensity during the extended monsoon is analyzed. The modulation patterns of the ER wave are shown for all eight phases and will be discussed in detail because of the notable influence far into the subtropics (Fig. 5). For the remaining waves only the wet phase (P5) and one neutral phase (P3) will be shown; the full figures showing all phases and maps with precipitation anomalies as measured and filtered by TRMM can be found in the supplemental material (Figs. S2–S12).

Although the composites are based on a local wave filtering for a reference location at 0°E, 5°–15°N, the ER wave shows significant and spatially coherent modulation patterns over most of northern tropical Africa. The eight phases give a clear picture of the propagation of the ER wave. As a largely independent dataset, rain gauge measurements confirm the significant influence over the entire continent. The wave exhibits significant modulation patterns that reach up to the Mediterranean Sea and to East Africa. The approximate wavelength is 8000 km; thus, it is dry over central and East Africa when wet anomalies persist over West Africa and vice versa. The modulation patterns as measured by TRMM are very similar to CHIRPS but more noisy and not as pronounced (Fig. S7); as expected from theory, weak symmetric signals at 10°S can be seen in several phases over the Atlantic Ocean. The modulation patterns of ER waves in Janicot et al. (2010, 2011) and Thiawa et al. (2017) are remarkably similar to the results of this composite study. The slightly eastward tilted precipitation pattern resembles tropical plumes regularly observed during the dry winter season (Knippertz and Martin 2005; Fröhlich et al. 2013). An analysis of the dynamical fields is needed to verify whether such a relation between tropical plumes and ER waves does in fact exist.

The remaining waves also show modulation patterns influencing all of northern tropical Africa (Fig. 6). The MJO modulates the precipitation over the entire African continent far into the subtropics up to the Mediterranean Sea and to East Africa (Figs. 6a,f; see also Figs. S2 and S8). Over the west coast, South Sudan, and central Africa, the modulation is weak. Over the complex East African terrain, the MJO seems to be out of phase. For the transition phases, a weak zonal dipole exists, with wet (dry) conditions over the tropical band and dry (wet) conditions over the Sahara. Weak anticorrelated wave patterns south of 5°N can be seen over the Atlantic Ocean (Fig. S8). The tilted precipitation anomalies over the Sahara as seen for the ER can also be observed for MJO waves, although this pattern is not as pronounced (P2 and P4; see Fig. S2). Over the Atlas Mountains, precipitation is enhanced during the wet phases and reduced during the dry phases (cf. Fig. S8). The TRMM-filtered composites suggest that the signal over the Gulf of Guinea precedes the signal over the continent.

MRG waves are rather confined to the filtered band between 5° and 15°N and lose their clear pattern over East Africa (Figs. 6b,g; see also Figs. S3 and S9). In the subtropics, only weak significant signals can be observed over the Maghreb region (P7; see Fig. S3). The approximate wavelength is >9000 km. An antisymmetric pattern in the Southern Hemisphere, as expected from theory, is observable with TRMM (Fig. S9) but not with CHIRPS due to the lack of data over oceans. Over central and East Africa, the antisymmetric pattern is weak.

Kelvin waves are an equatorial phenomenon. This is the reason why the modulation also extends to 10°S but

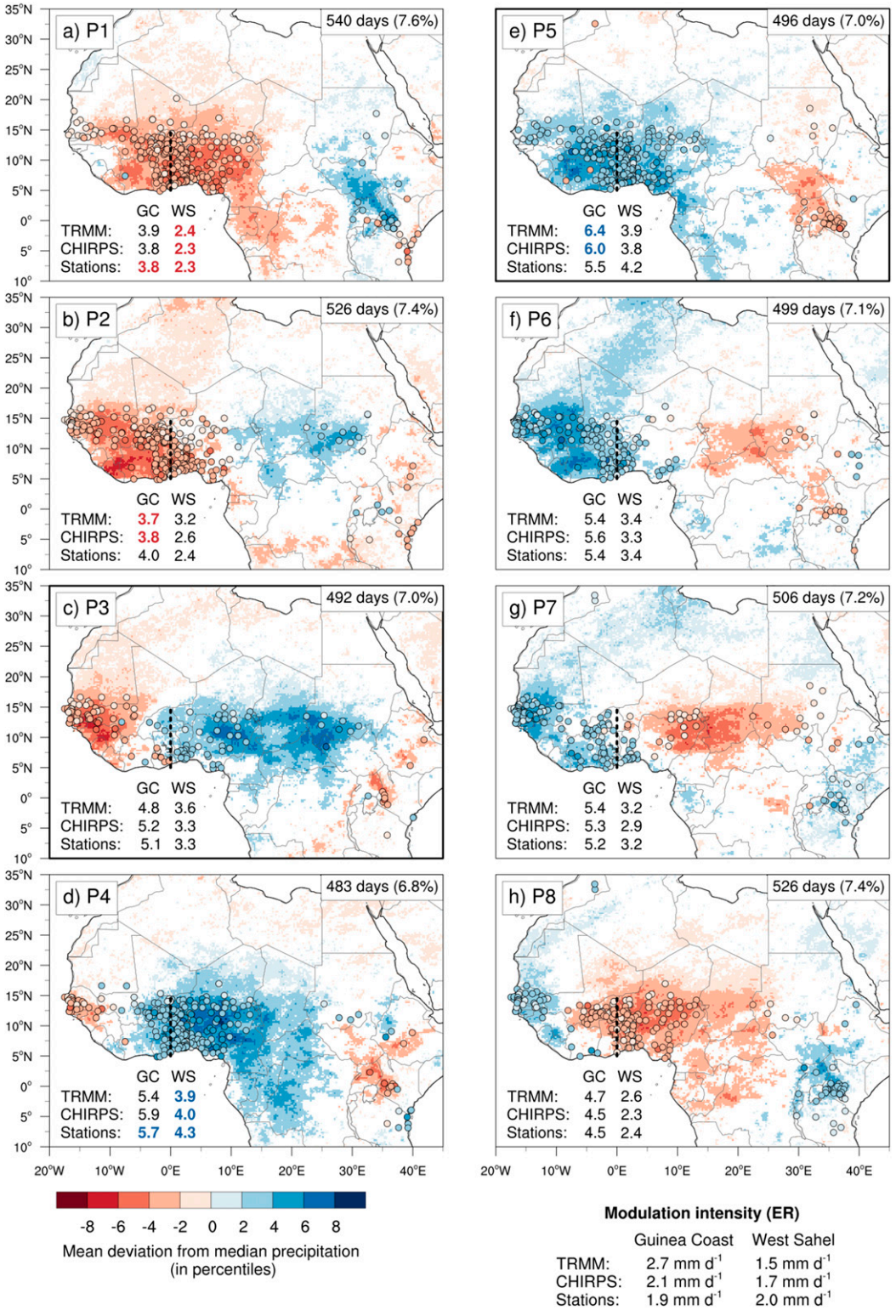

FIG. 5. Rainfall composite for days with significant ER wave signal, based on OLR anomalies over 5°–15°N, 0°E (dashed line), for CHIRPS (shading) and KASS-D (circles; both 1981–2013) during the extended monsoon season (April–October). As calculated with a bootstrap test, nonsignificant anomalies ($p > 0.05$) are left white for the CHIRPS data, KASS-D stations that are nonsignificant are not shown. The number of days used for the composites and the fraction of days per season during each phase is given in the top right of the plot. The numbers in the bottom left of the subpanels states the mean observed rainfall in all three rainfall datasets for the given phases (TRMM period: 1998–2013) within the Guinea Coast and West Sahel (black boxes). The modulation intensity, measured as the difference between the mean rainfall amount in the wettest (blue number) and driest phase (red number), is summarized at bottom right.

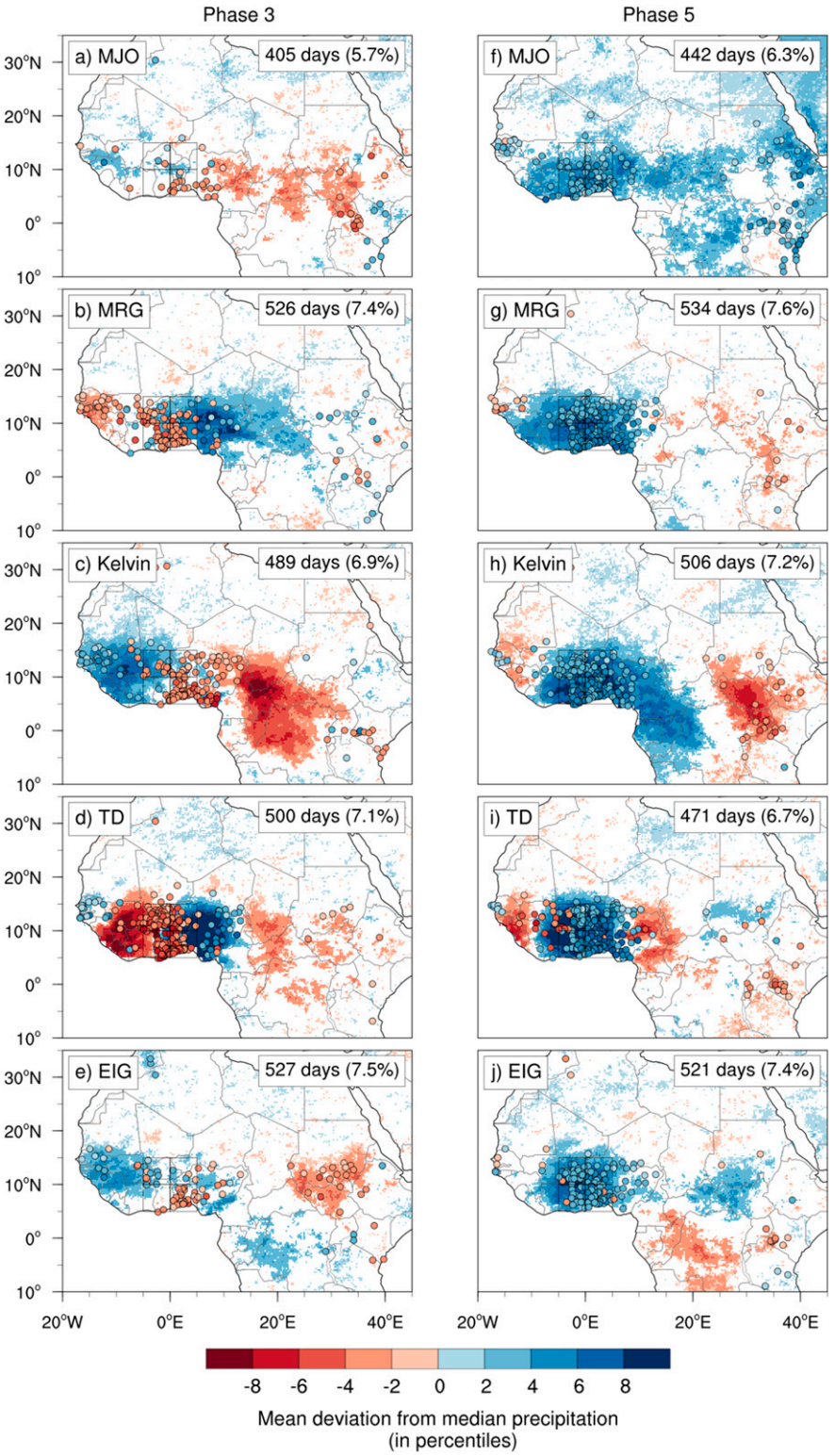

FIG. 6. As in Fig. 5, but for all waves and (a)–(e) phase 3 (neutral phase) and (f)–(j) phase 5 (wet phase). Plots showing all phases are provided in the supplemental material (Figs. S2–S6). For abbreviations of wave names, see Table 1.

not to the north of the filtered band at 15°N (Figs. 6c,h; see also Figs. S4 and S10). The precipitation patterns are well defined and blur out over the eastern part of the continent. As a side remark, Kelvin waves might also locally modulate the land–sea breeze as indicated by a modulation that is out of phase at several coastal stations (P4 and P8; Fig. S4).

TDs are most dominant over West Africa (Figs. 6d,i; see also Figs. S5 and S11). The wave signal weakens east of 10°E. The influence is also mostly confined to the filtered area between 5° and 15°N. A weak anticorrelation with precipitation in the Sahara can be observed. Over the Atlantic the precipitation pattern tilts in a northeast–southwest direction (Fig. S11). The average wavelength is about 2500 km.

EIG waves show a weaker and more complex modulation pattern compared with the previous waves (Figs. 6e,j; see also Figs. S6 and S12). The modulation is strongest over West Africa, equatorial central Africa, and South Sudan. Consistent with theory, antisymmetric rainfall patterns are evident in the Southern Hemisphere, although the anticorrelated rainfall regions are shifted northward and centered around 5°S. Very weak significant anticorrelated precipitation anomalies farther in the north could be an indication of a contamination by higher-order (e.g., $n = 1$, $n = 2$) EIG waves. Further investigations are needed to better understand the involved mechanisms of triggering, propagation, and coupling of EIG waves to precipitation. Rain gauge observations do not match the CHIRPS dataset well due to a phase shift between both datasets, which will be the topic of the following section.

A detailed comparison of modulation patterns and the associated circulation of all wave types with theory will follow in the second part of this study.

d. Modulation intensity

The modulation intensity was measured in absolute rainfall. Figure 7 shows the mean precipitation in the Guinea Coast and West Sahel boxes during the eight phases as measured by CHIRPS, TRMM, and KASS-D. Rainfall varies considerably between the different phases of all waves. Additionally, it can be seen that TDs and Kelvin waves have the strongest impact on absolute rainfall anomalies, followed by MRG and ER waves. Despite the known deficiencies of the datasets (Funk et al. 2015; Maggioni et al. 2016), the observed amplitudes agree well for all three datasets.

In a more detailed analysis, gauge observations will be analyzed for the transition season and the full monsoon season. Figure 8 shows the distribution of mean modulation for all stations in the West Sahel and Guinea Coast box as the difference of modulation intensities

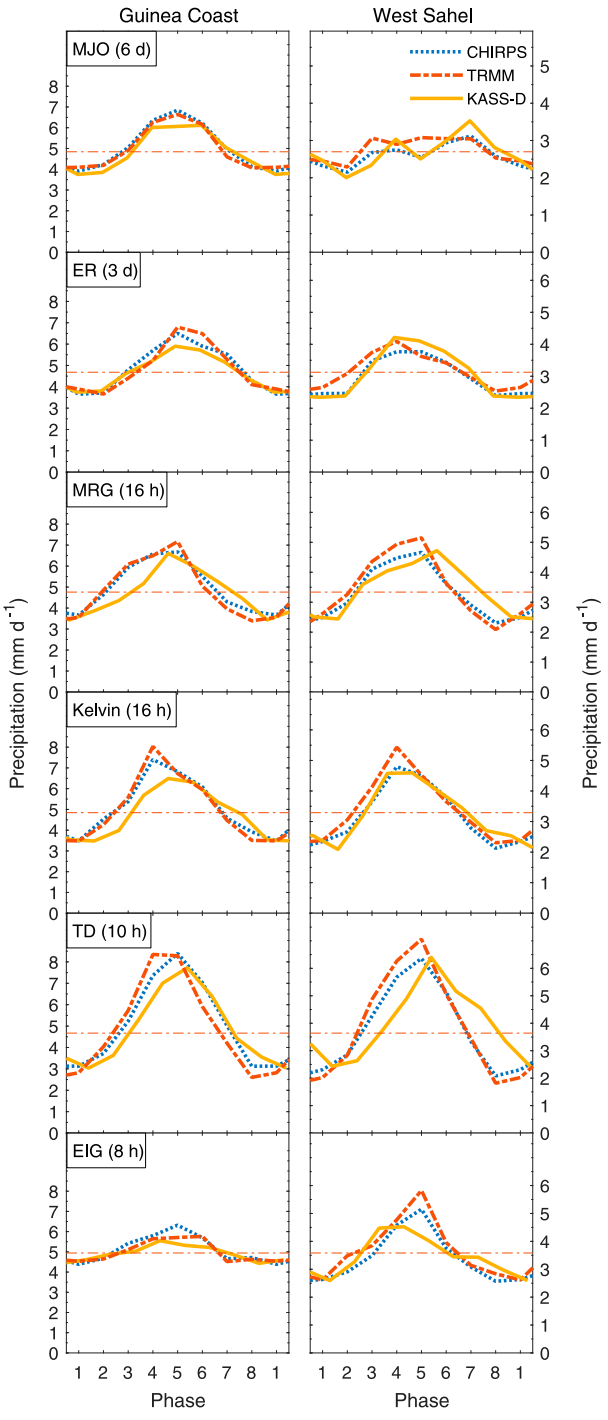

FIG. 7. Mean precipitation in the eight phases in (left) the Guinea Coast box and (right) the West Sahel box in CHIRPS (1981–2013; blue dotted line), TRMM (1998–2013; red dashed line), and KASS-D (1981–2013; yellow solid line) during the extended monsoon season (April–October). Because KASS-D lags the other datasets by 6 h, the curve has been shifted using the mean duration of one phase (in parentheses). See section 2f for more detail. Note that the *y* axis has been scaled with the mean TRMM precipitation during all days with an active wave, which is indicated by the horizontal red line.

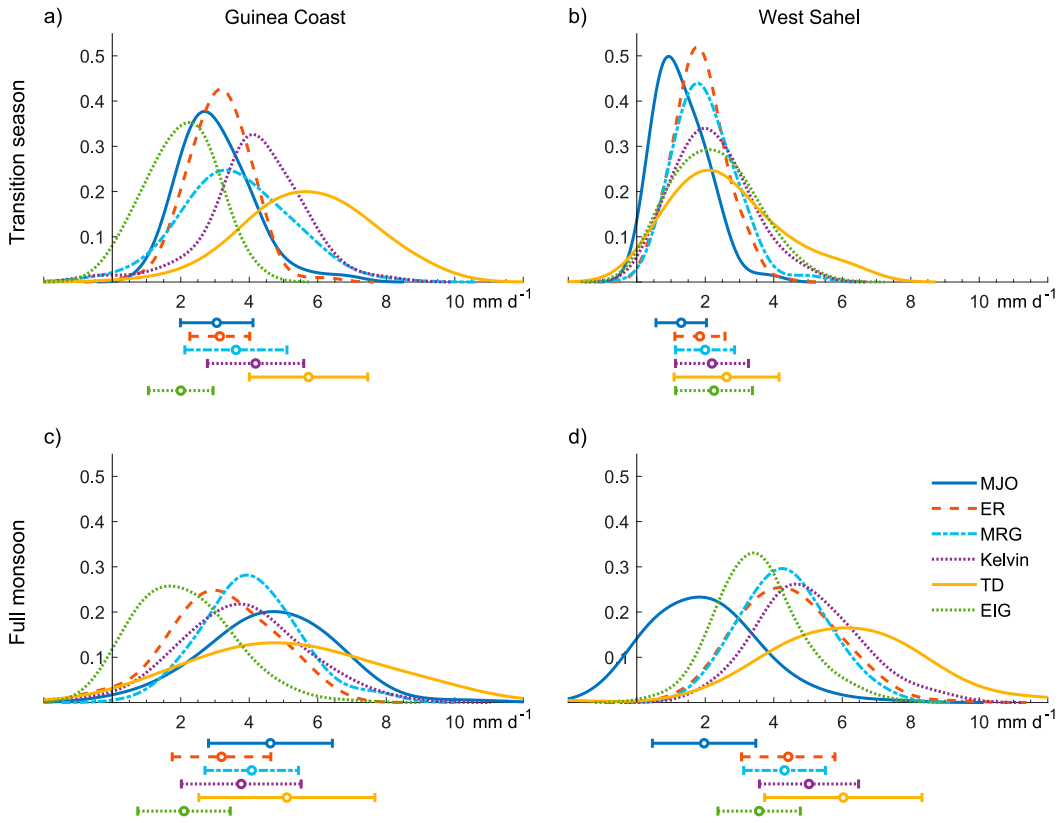

FIG. 8. Modulation of rainfall by tropical waves in the (a),(c) Guinea Coast (5°W–5°E, 5°–10°N) and (b),(d) West Sahel (5°W–5°E, 10°–15°N) during (top) the transition season (April–June; October) and (bottom) the full monsoon season (July–September) as measured by rain gauges in KASS-D. Dates in wet and dry phases of the tropical waves were obtained by filtering OLR in a Guinean (5°–10°N) and Sahelian band (10°–15°N) from 1979 to 2013. As a metric for the modulation intensity, the difference of the mean precipitation during wet phases and dry phases was calculated for all stations (Guinea $n = 112$, Sahel $n = 129$). From these stations an empirical probability density function was derived using kernel density estimation. Lines below the axis show the mean and standard deviation of the corresponding modulation intensity for each wave. For abbreviations of wave names, see Table 1.

during the wet and dry phases of the waves. As a side remark, it can be noted that negative modulation intensities can be observed, which means that less rain at single stations falls during the wet phase and vice versa. These cases are likely related to local factors such as orography (cf. Figs. 5 and 6 and section 3f) and random errors. The corresponding plot in quantile anomalies can be found in the supplemental material (Fig. S13).

During the transition season, rainfall at the Guinea Coast is strongly modulated by tropical waves (Fig. 8a). Descending in order, the mean modulation intensities are 5.7 (TD), 4.2 (Kelvin), 3.6 (MRG), 3.1 (ER), 3.0 (MJO), and 2.0 mm day^{-1} (EIG). The standard deviations lie between 0.8 mm day^{-1} for ER and 1.7 mm day^{-1} for TD. The West Sahel is still relatively dry during the transition season (Fig. 3a). Therefore, the influence of tropical waves is weak, amounting to only 1.3–2.6 mm day^{-1} for all waves (Fig. 8b).

In the full monsoon season, the modulation at the Guinea Coast is similar to the transition season (Fig. 8c). The mean modulation intensities amount to 5.9 (TD), 4.6 (MJO), 4.1 (MRG), 3.7 (Kelvin), 3.2 (ER), and 2.1 mm day^{-1} (EIG). A noteworthy difference to the transition season is a stronger modulation by the MJO, although the MJO activity itself is weaker during the full monsoon (Fig. 4). The standard deviations are higher than during the transition season due to the high gradient of rainfall at the Guinea Coast during the monsoon season (Fig. 3). Surprisingly, all CCEWs are as strong as or even stronger in the West Sahel (Fig. 8d) than over the Guinea Coast (Fig. 8c), although the strongest influence of equatorial waves would be expected near the equator from theory. The mean modulation intensities are 6.0 (TD), 5.0 (Kelvin), 4.4 (ER), 4.3 (MRG), 3.5 (EIG), and 2.0 mm day^{-1} (MJO). For both regions, the largest standard deviation is seen in the modulation

intensity for TD. Several stations record a modulation intensity of more than 8 mm day.

e. *Relative contributions to precipitation*

To understand the relative contribution of the tropical waves to rainfall variability on different time scales, the wave filtered precipitation was correlated with temporally aggregated raw precipitation (Figs. 9–11). The squared correlation is calculated as an estimation of the explained variance of raw precipitation by the tropical waves. All waves significantly modulate precipitation over the Sahel and Guinean bands. Using this correlation analysis, we can obtain a more detailed overview over the longitudinally varying modulation strength as well as the relative contribution to rainfall variability on different time scales. Interactions between different waves are not taken into account, so the sum can be seen as the maximum that can be explained by the six tropical waves combined. During the transition season, the Sahel band receives very little rainfall (Fig. 3) and the influence of tropical waves is comparatively weak (Figs. 4 and 8b). Thus, a figure for the Sahel band during the transition is not discussed here but is available in the supplemental material (Fig. S14).

For both seasons and both bands, we can observe that the influence of tropical waves depends on the time scale and varies substantially with location and season. As expected, waves in shorter period bands generally dominate the rainfall variability on shorter time scales, whereas the longer time scales are governed by slower waves. It should be noted that a specific wave modulates precipitation at the accumulation period less than or equal to half the wave period. At accumulation times equal to one period (and longer), the enhanced and suppressed phase cancel each other out and thus no correlation can be seen anymore at this time scale.

The Guinea band exhibits the strongest modulation on the daily time scale during the transition season (Fig. 9). Here, the TD and Kelvin waves have the strongest impact. Between the Cameroon Line (12°E) and the Ethiopian Highlands (38°E), rainfall variability is dominated by Kelvin waves. On the time scale of three days, MJO, ER, and Kelvin waves are approximately equally important. The influence of TDs is not evident any more on this time scale. On the weekly time scale, ER and MJO remain as the only contributors to rainfall variability. On the short subseasonal time scale (20 days), the MJO is the remnant major source of rainfall variability locally explaining 10%–20% of rainfall variability over West Africa and up to 20%–30% over the Horn of Africa. A stronger influence of the MJO on central African precipitation during the spring season was documented by Berhane et al. (2015).

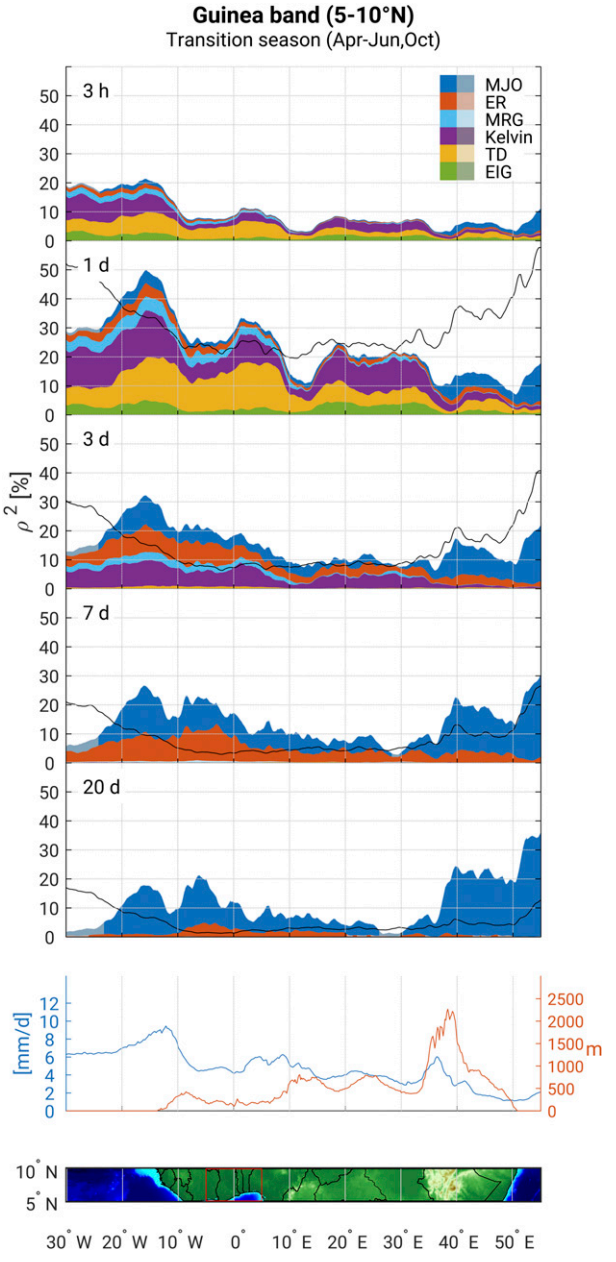

FIG. 9. (top) Relative importance of tropical wave signals for TRMM precipitation (1998–2016) on different time scales over (bottom) the Guinean band (5°–10°N) during the transition season (April–June and October). Explained variance is estimated by the squared correlations of the wave signal with raw precipitation. Lines are stacked on top of each other, such that the sum of all lines can be understood as the maximum variance explained by all wave types. Significant correlations ($p < 0.05$) are indicated with saturated colors. The black solid line shows the variance of precipitation at the specific time scale as percentage of the total variance in the raw data (3 h). Band-averaged daily precipitation and surface height is given in the second lowest panel.

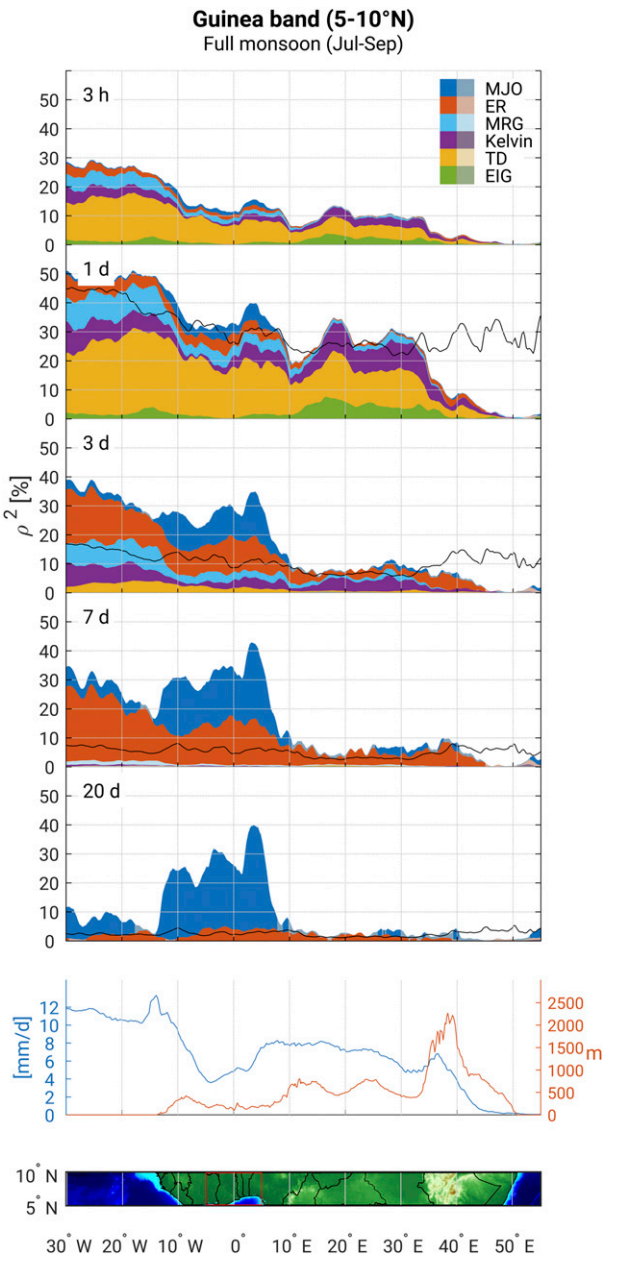

FIG. 10. As in Fig. 9, but during the full monsoon season (July–September).

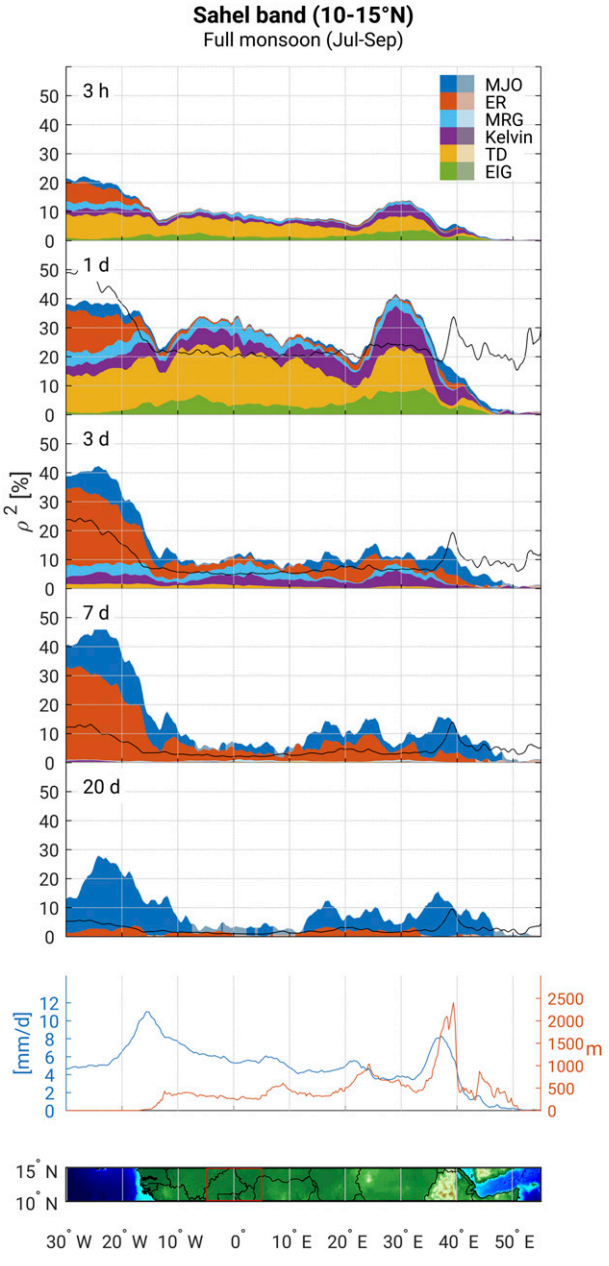

FIG. 11. As in Fig. 9, but over the Sahelian band (10°–15°N) and during the full monsoon season (July–September).

During the full monsoon, the TDs gain importance for rainfall variability in the Guinea band. On the daily time scale, they explain up to 30% of the variability over West Africa (Fig. 10). This is consistent with Dickinson and Molinari (2000) and Lavaysse et al. (2006), who found numbers of the same order for AEWs. The importance of AEWs on daily precipitation increases westward, which might be attributed to the barotropic–baroclinic growth they experience on the way toward the Atlantic (Charney and Stern 1962; Thorncroft and Hoskins 1994; Hsieh and Cook 2005). The influence of Kelvin waves is reduced compared to the transition season, but still explains up to 10% over central Africa, slightly less than what is recorded by Mekonnen and Thorncroft (2016). EIG and MRG waves gain importance west of 10°W on the time scale of 1–3 days. On the synoptic time scale (3–7 days), ER contribute about 10%–20% to rainfall variability. The main influence of the MJO on the short subseasonal time scale (7–20 days) lies within the West

African monsoon region, explaining locally more than one-third of rainfall variability. There is no significant influence of the MJO on central and East African rainfall.

In the Sahel band, TD are the dominant wave on the 3-hourly to daily time scale, explaining up to 20% of the rainfall variability during the full monsoon (Fig. 11). A large portion of rainfall variability is concentrated on time scales longer than three days off the west coast of Africa (black line). From three to seven days, ER waves are a large contributor to rainfall variability in this region, explaining up to one-third of rainfall variability. On longer time scales (20 days), only the MJO signal contributes to rainfall variability over the Atlantic Ocean and parts of East Africa. A more pronounced modulation of the MJO in the Guinea band than in the Sahel band was also found by Gu (2009) and Pohl et al. (2009).

The QBZD and the Sahel mode operate on the time scale of 10–25 days. Mounier et al. (2008) showed that the QBZD has a stationary component and suggested Kelvin waves as triggers for the QBZD. The present correlation analysis suggests that Kelvin waves do not explain rainfall variability on time scales longer than seven days. It has to be noted, though, that the correlation analysis cannot take into account cases when Kelvin waves trigger the QBZD, which then affects longer time scales. The Sahel mode is mainly associated with ER waves (Janicot et al. 2010). ER explain a substantial portion on the weekly time scale; yet, the present analysis suggest, that ''pure'' ER waves, as derived from the shallow water equations, are barely relevant on the time scale of 20 days (Figs. 9–11). The correlation analysis again might not capture cases when on a longer time scale, MJO events over the Indian ocean trigger single ER and Kelvin waves that meet over the African continent as suggested by Matthews (2000, 2004). The present analysis should be understood as an account of how much variability can be explained by the respective wavenumber–frequency bands, independent of more complex wave interactions.

f. *The role of orography*

The effect of orography on the propagation of the MJO and the diurnal cycle of precipitation over the Maritime Continent has been widely discussed (e.g., Inness and Slingo 2006; Peatman et al. 2014; Tseng et al. 2017; Sakaeda et al. 2017; Tan et al. 2018). Over northern tropical Africa, several tropical waves also appear to be influenced by the presence of orography. Both latitudinal bands show a reduced influence of tropical waves over orography (Figs. 9–11). In the Guinea band, Kelvin waves and EIG are reduced after the passage of the Guinea Highlands (12°W), over the Cameroon Line (12°E) and the Ethiopian Highlands (38°E). The reduced modulation of TDs is evident over the Guinea Highlands (12°W), Cameroon Line (12°E), the Bongo Massif (25°E), and the Ethiopian Highlands (38°E). In the Sahel band, the influence of tropical waves is reduced over the Guinea Highlands (12°W), the Jos Plateau (8°E), the Darfur Mountains (23°E), and the Ethiopian Highlands (38°E). A reduced modulation over the Cameroon Line can also be seen in Figs. 5 and 6 and Figs. S4 and S5 for the ER, Kelvin waves, and TDs. In general, the reduced effect of tropical waves over orography is more pronounced on the daily and subdaily time scale, where the waves compete directly with diurnal circulations, and is on the order of 50%. The effect of orography, and the Ethiopian Highlands in particular, on Kelvin waves has been documented by Matthews (2000). Kelvin waves encountering orography can be deflected away from the equator similar to coastal Kelvin waves in the ocean (Gill 1977; Hsu and Lee 2005). Additionally, the orographic lifting and frictionally induced lower-tropospheric convergence create a phase shift (Hsu and Lee 2005). Figure S4 also suggests that convection over the Cameroon Line is shifted by one phase. AEWs preferably form in the lee of mountain ranges, where vorticity is increased (Mozer and Zehnder 1996), and in consequence of mesoscale convective systems that have been triggered over the mountains (Mekonnen et al. 2006; Thorncroft et al. 2008). The present study illustrates how orography significantly reduces the modulation of tropical waves over northern tropical Africa.

g. *Wave interactions*

Finally, interactions between different types of tropical waves over the two case study regions Guinea Coast and West Sahel are examined. Only the results for the Guinea Coast are presented here because the results are very similar for both regions. Figure 12 shows the interaction between a primary wave and a secondary wave for all analyzed wave types in the Guinea Coast. The primary modulation in the Guinea Coast (shown on the diagonal) reflects the pattern already seen in Fig. 4. The modulation by a second wave is seen in the entries off the diagonal of the matrix. The magnitude of the secondary modulation depends on the magnitude of the primary modulation and is strongest for TDs. In many cases, waves superimpose constructively. The wave activity is generally further enhanced when a primary wave in its positive phase is modulated by a second wave in a positive phase (top-left quarter). Similarly, primary waves in a negative phase modulated by a negative second wave result in a further suppression (bottom-right

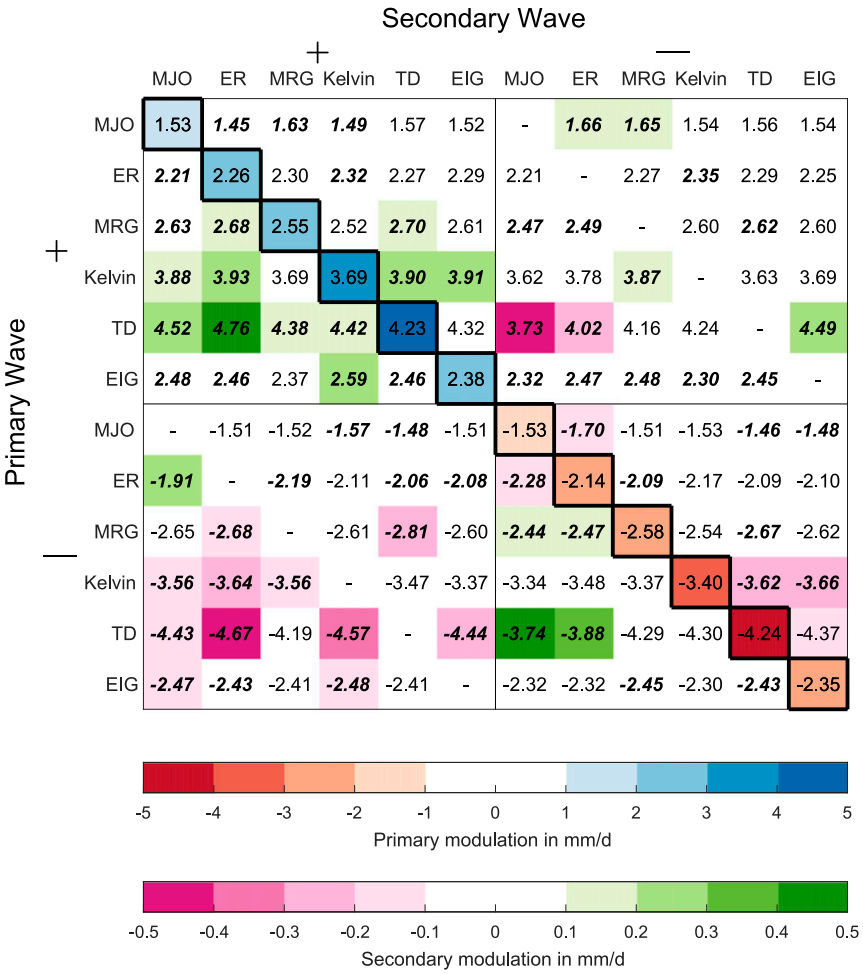

FIG. 12. Interaction of different wave types in the Guinea Coast box. The mean or primary modulation of each wave measured as the mean wave filtered TRMM precipitation is given on the diagonal. Cases with a wave activity exceeding $\pm 1\sigma$ are defined as wet (−) and dry (+) phases. The superposition of a secondary wave is measured as the primary wave signal conditional on the occurrence of a secondary wave. Significant deviations from mean modulation are marked bold and italics ($p < 5\%$). See section 2h for more details.

quarter). Two interesting exceptions of this wave superpositions can be seen for TDs and MRG waves. Here, a modulation of the negative primary wave by a negative ER wave or MJO result in a more moderate modulation. Similarly, nonlinear wave superpositions are evident when a positive wave is superimposed with a negative wave (top-left and bottom-right quarters). This means that both low-frequency waves in their wet phases amplify the high-frequency waves and suppress them in the dry phase. The analysis for the West Sahel reveals similar patterns (Fig. S15). A dominant difference is a missing modulation of TD by the dry phases of ER and MJO waves.

According to theory, equatorial waves behave as linear or independent solutions of the shallow-water system (Matsuno 1966). This is, of course, an idealized view; the basic analysis of wave interactions presented here suggest that also the dry phases of TDs during the passage of the suppressed phase of MJO and ER events are significantly weaker. The superposition of AEWs and MJO events was also analyzed by Ventrice et al. (2011). Decreased AEW activity was found when the MJO is active over the western Pacific and Atlantic, whereas AEW activity was enhanced in phases where the MJO is active over Africa and the Indian Ocean. The superposition of MJO, Kelvin, and ER waves over Vietnam was analyzed in detail by van der Linden et al. (2016). The presented results suggest complex superpositions that require to be analyzed in more detail.

4. Conclusions

The impact of tropical waves on rainfall variability over northern tropical Africa has long been known but the relative influences of the different tropical wave types have never been quantified for this region. As previous studies applied different methodologies and datasets, a systematic comparison of the results has been difficult. This study closes this gap and gives a first comprehensive and systematic account of the influence of all major tropical wave types for daily to intraseasonal rainfall variability over northern tropical Africa. A consistent method was applied to all waves and modulation intensities were quantified comparing two satellite datasets and data from a dense rain gauge network. The new quantification of rainfall anomalies using quantile anomalies made it possible to compare the influence on precipitation in different climatic zones and revealed influences deep into the subtropics. All analyzed waves were found to significantly modulate rainfall variability in the monsoon system on different temporal scales. The main findings are as follows:

- Equatorial waves contribute most to rainfall variability over northern tropical Africa in the area of the seasonal rainfall maximum. TDs and Kelvin waves explain the overall highest variability followed equally by MRG and ER waves.
- Precipitation patterns of tropical waves are mainly confined to the tropics. Notably, the influence of MJO and ER waves reaches deep into the subtropics and their modulation patterns resemble tropical plumes (Knippertz and Martin 2005; Fröhlich et al. 2013). The different datasets show comparable modulation intensities varying from less than 2 to above 7 mm day^{-1} depending on the wave type.
- Tropical waves modulate precipitation on different time scales. The influence varies with location and season. On the 3-hourly to daily time scale, TDs and Kelvin waves are the dominant wave types. On longer time scales (7–20 days), only the MJO and ER remain as modulating factors for rainfall variability. For the first time, this study analyzed the influence of EIG on northern Africa. Over central and East Africa, EIG waves explain 5%–10% of rainfall variability on the daily time scale. The rainfall modulation by several tropical waves is reduced over orography.
- Tropical waves superimpose and interact with each other. During their wet phases, the low-frequency waves (MJO and ER) amplify the high-frequency TDs and MRG waves and suppress them in their dry phase.

Several open questions remain. The present study only gives an observational account of tropical waves. It remains unclear how the waves influence the dynamic and thermodynamic environment as well as how interactions with the West African monsoon system work. A follow-up paper will deal with these open questions in order to get a better understanding how the different waves differ in the way they modulate the dynamics and thermodynamics of the West African monsoon.

This study emphasizes the need of an adequate representation of tropical waves in NWP models for weather prediction over northern tropical Africa. Further research is needed to assess and improve the prediction of the correct phase and intensity of the waves. Additionally, the statistical relationships found here indicate that, besides conventional NWP models, statistical forecast models including tropical waves may provide useful predictions, bearing in mind that so far global NWP models have failed to reliably predict precipitation over this region (Vogel et al. 2018). First promising results have already been achieved by the authors and are currently being investigated in more detail.

Finally, the results stress the importance of tropical waves for operational forecasting of precipitation on different time scales for this region. The presented new visualization showing the contribution of tropical waves on precipitation variability on different time scales is useful for weather forecasters to determine the relevance of different waves for their region depending on the analyzed time scale. Further research and collaboration with national and pan-African weather agencies should be encouraged to foster the knowledge transfer to local societies.

Acknowledgments. The research leading to these results has been accomplished within project C2 ''Prediction of wet and dry periods of the West African Monsoon'' of the Transregional Collaborative Research Center SFB/TRR 165 ''Waves to Weather'' funded by the German Science Foundation (DFG). The authors thank George Kiladis and two anonymous reviewers whose comments helped to improve and clarify this manuscript. We also thank Tilmann Gneiting for discussions and comments on draft versions of the paper. The authors also thank various colleagues and weather services that have over the years contributed to the enrichment of the KASS-D database; special thanks go to Robert Redl for creating the underlying software. The authors also thank Roderick van der Linden for providing code that was further developed to filter the waves and create the composite plots. Finally, we thank Carl Schreck III for providing the filtering function ''kf_filter.''

REFERENCES

Alaka, G. J., and E. D. Maloney, 2012: The influence of the MJO on upstream precursors to African easterly waves. *J. Climate*, **25**, 3219–3236, https://doi.org/10.1175/JCLI-D-11-00232.1.

——, and ——, 2014: The intraseasonal variability of African easterly wave energetics. *J. Climate*, **27**, 6559–6580, https://doi.org/10.1175/JCLI-D-14-00146.1.

——, and ——, 2017: Internal intraseasonal variability of the West African monsoon in WRF. *J. Climate*, **30**, 5815–5833, https://doi.org/10.1175/JCLI-D-16-0750.1.

Arkin, P. A., and P. E. Ardanuy, 1989: Estimating climatic-scale precipitation from space: A review. *J. Climate*, **2**, 1229–1238, https://doi.org/10.1175/1520-0442(1989)002<1229:ECSPFS>2.0.CO;2.

Berhane, F., B. Zaitchik, and H. S. Badr, 2015: The Madden–Julian oscillation's influence on spring rainy season precipitation over equatorial West Africa. *J. Climate*, **28**, 8653–8672, https://doi.org/10.1175/JCLI-D-14-00510.1.

Castanheira, J. M., and C. A. F. Marques, 2015: Convectively coupled equatorial-wave diagnosis using three-dimensional normal modes. *Quart. J. Roy. Meteor. Soc.*, **141**, 2776–2792, https://doi.org/10.1002/qj.2563.

Charney, J. G., and M. E. Stern, 1962: On the stability of internal baroclinic jets in a rotating atmosphere. *J. Atmos. Sci.*, **19**, 159–172, https://doi.org/10.1175/1520-0469(1962)019<0159:OTSOIB>2.0.CO;2.

Chauvin, F., R. Roehrig, and J.-P. Lafore, 2010: Intraseasonal variability of the Saharan heat low and its link with midlatitudes. *J. Climate*, **23**, 2544–2561, https://doi.org/10.1175/2010JCLI3093.1.

Dias, J., and G. N. Kiladis, 2016: The relationship between equatorial mixed Rossby–gravity and eastward inertio-gravity waves. Part II. *J. Atmos. Sci.*, **73**, 2147–2163, https://doi.org/10.1175/JAS-D-15-0231.1.

Dickinson, M., and J. Molinari, 2000: Climatology of sign reversals of the meridional potential vorticity gradient over Africa and Australia. *Mon. Wea. Rev.*, **128**, 3890–3900, https://doi.org/10.1175/1520-0493(2001)129<3890:COSROT>2.0.CO;2.

FAO, 2016: AQUASTAT. FAO, http://www.fao.org/nr/aquastat.

Fink, A. H., and P. Speth, 1997: Some potential forcing mechanisms of the year-to-year variability of the tropical convection and its intraseasonal (25–70-day) variability. *Int. J. Climatol.*, **17**, 1513–1534, https://doi.org/10.1002/(SICI)1097-0088(19971130)17:14<1513::AID-JOC210>3.0.CO;2-U.

——, and A. Reiner, 2003: Spatiotemporal variability of the relation between African easterly waves and West African squall lines in 1998 and 1999. *J. Geophys. Res.*, **108**, 4332, https://doi.org/10.1029/2002JD002816.

——, and Coauthors, 2017: Mean climate and seasonal cycle. *Meteorology of Tropical West Africa: The Forecasters' Handbook*, D. J. Parker and M. Diop-Kane, Eds., John Wiley & Sons, 1–39, https://doi.org/10.1002/9781118391297.ch1.

Freedman, D., and P. Diaconis, 1981: On the histogram as a density estimator: L2 theory. *Z. Wahrscheinlichkeitstheorie Verw. Geb.*, **57**, 453–476, https://doi.org/10.1007/BF01025868.

Fröhlich, L., P. Knippertz, A. H. Fink, and E. Hohberger, 2013: An objective climatology of tropical plumes. *J. Climate*, **26**, 5044–5060, https://doi.org/10.1175/JCLI-D-12-00351.1.

Funk, C., and Coauthors, 2015: The Climate Hazards Infrared Precipitation with Stations—A new environmental record for monitoring extremes. *Sci. Data*, **2**, 150066, https://doi.org/10.1038/sdata.2015.66.

Gill, A. E., 1977: Coastally trapped waves in the atmosphere. *Quart. J. Roy. Meteor. Soc.*, **103**, 431–440, https://doi.org/10.1002/qj.49710343704.

Gonzales-Fuentes, L., K. Barbé, L. Barford, L. Lauwers, and L. Philips, 2015: A qualitative study of probability density visualization techniques in measurements. *Measurement*, **65**, 94–111, https://doi.org/10.1016/j.measurement.2014.12.022.

Gu, G., 2009: Intraseasonal variability in the equatorial Atlantic–West Africa during March–June. *Climate Dyn.*, **32**, 457–471, https://doi.org/10.1007/s00382-008-0428-0.

Holder, C. T., S. E. Yuter, A. H. Sobel, and A. R. Aiyyer, 2008: The mesoscale characteristics of tropical oceanic precipitation during Kelvin and mixed Rossby–gravity wave events. *Mon. Wea. Rev.*, **136**, 3446–3464, https://doi.org/10.1175/2008MWR2350.1.

Hsieh, J.-S., and K. H. Cook, 2005: Generation of African easterly wave disturbances: Relationship to the African easterly jet. *Mon. Wea. Rev.*, **133**, 1311–1327, https://doi.org/10.1175/MWR2916.1.

Hsu, H.-H., and M.-Y. Lee, 2005: Topographic effects on the eastward propagation and initiation of the Madden–Julian oscillation. *J. Climate*, **18**, 795–809, https://doi.org/10.1175/JCLI-3292.1.

Huang, P., and R. Huang, 2011: Climatology and interannual variability of convectively coupled equatorial waves activity. *J. Climate*, **24**, 4451–4465, https://doi.org/10.1175/2011JCLI4021.1.

Huffman, G. J., and Coauthors, 2007: The TRMM Multisatellite Precipitation Analysis (TMPA): Quasi-Global, Multiyear, Combined-Sensor Precipitation Estimates at Fine Scales. *J. Hydrometeor.*, **8**, 38–55, https://doi.org/10.1175/JHM560.1.

Inness, P. M., and J. M. Slingo, 2006: The interaction of the Madden–Julian oscillation with the Maritime Continent in a GCM. *Quart. J. Roy. Meteor. Soc.*, **132**, 1645–1667, https://doi.org/10.1256/qj.05.102.

Janicot, S., F. Mounier, N. M. J. Hall, S. Leroux, B. Sultan, and G. N. Kiladis, 2009: Dynamics of the West African monsoon. Part IV: Analysis of 25–90-day variability of convection and the role of the Indian monsoon. *J. Climate*, **22**, 1541–1565, https://doi.org/10.1175/2008JCLI2314.1.

——, ——, S. Gervois, B. Sultan, and G. N. Kiladis, 2010: The dynamics of the West African monsoon. Part V: The detection and role of the dominant modes of convectively coupled equatorial Rossby waves. *J. Climate*, **23**, 4005–4024, https://doi.org/10.1175/2010JCLI3221.1.

——, and Coauthors, 2011: Intraseasonal variability of the West African monsoon. *Atmos. Sci. Lett.*, **12**, 58–66, https://doi.org/10.1002/asl.280.

Kikuchi, K., and B. Wang, 2010: Spatiotemporal wavelet transform and the multiscale behavior of the Madden–Julian oscillation. *J. Climate*, **23**, 3814–3834, https://doi.org/10.1175/2010JCLI2693.1.

Kiladis, G. N., M. C. Wheeler, P. T. Haertel, K. H. Straub, and P. E. Roundy, 2009: Convectively coupled equatorial waves. *Rev. Geophys.*, **47**, RG2003, https://doi.org/10.1029/2008RG000266.

——, J. Dias, K. H. Straub, M. C. Wheeler, S. N. Tulich, K. Kikuchi, K. M. Weickmann, and M. J. Ventrice, 2014: A comparison of OLR and circulation-based indices for tracking the MJO. *Mon. Wea. Rev.*, **142**, 1697–1715, https://doi.org/10.1175/MWR-D-13-00301.1.

——, ——, and M. Gehne, 2016: The relationship between equatorial mixed Rossby–gravity and eastward inertio-gravity waves. Part I. *J. Atmos. Sci.*, **73**, 2123–2145, https://doi.org/10.1175/JAS-D-15-0230.1.

Knippertz, P., and J. E. Martin, 2005: Tropical plumes and extreme precipitation in subtropical and tropical West Africa. *Quart. J. Roy. Meteor. Soc.*, **131**, 2337–2365, https://doi.org/10.1256/qj.04.148.

——, and Coauthors, 2017: A meteorological and chemical overview of the DACCIWA field campaign in West Africa in

June–July 2016. *Atmos. Chem. Phys.*, **17**, 10 893–10 918, https://doi.org/10.5194/acp-17-10893-2017.

Laing, A. G., R. E. Carbone, and V. Levizzani, 2011: Cycles and propagation of deep convection over equatorial Africa. *Mon. Wea. Rev.*, **139**, 2832–2853, https://doi.org/10.1175/2011MWR3500.1.

Lavaysse, C., A. Diedhiou, H. Laurent, and T. Lebel, 2006: African easterly waves and convective activity in wet and dry sequences of the West African monsoon. *Climate Dyn.*, **27**, 319–332, https://doi.org/10.1007/s00382-006-0137-5.

Lavender, S. L., and A. J. Matthews, 2009: Response of the West African monsoon to the Madden–Julian oscillation. *J. Climate*, **22**, 4097–4116, https://doi.org/10.1175/2009JCLI2773.1.

Liebmann, B., and C. A. Smith, 1996: Description of a complete (interpolated) outgoing longwave radiation dataset. *Bull. Amer. Meteor. Soc.*, **77**, 1275–1277.

Lubis, S. W., and C. Jacobi, 2015: The modulating influence of convectively coupled equatorial waves (CCEWs) on the variability of tropical precipitation. *Int. J. Climatol.*, **35**, 1465–1483, https://doi.org/10.1002/joc.4069.

Madden, R. A., and P. R. Julian, 1971: Detection of a 40–50 day oscillation in the zonal wind in the tropical Pacific. *J. Atmos. Sci.*, **28**, 702–708, https://doi.org/10.1175/1520-0469(1971)028<0702:DOADOI>2.0.CO;2.

Maggioni, V., P. C. Meyers, and M. D. Robinson, 2016: A review of merged high-resolution satellite precipitation product accuracy during the Tropical Rainfall Measuring Mission (TRMM) era. *J. Hydrometeor.*, **17**, 1101–1117, https://doi.org/10.1175/JHM-D-15-0190.1.

Matsuno, T., 1966: Quasi-geostrophic motions in the equatorial area. *J. Meteor. Soc. Japan*, **44**, 25–44, https://doi.org/10.2151/jmsj1965.44.1_25.

Matthews, A. J., 2000: Propagation mechanisms for the Madden–Julian oscillation. *Quart. J. Roy. Meteor. Soc.*, **126**, 2637–2651, https://doi.org/10.1002/qj.49712656902.

——, 2004: Intraseasonal variability over tropical Africa during northern summer. *J. Climate*, **17**, 2427–2440, https://doi.org/10.1175/1520-0442(2004)017<2427:IVOTAD>2.0.CO;2.

Mayr, H. G., J. G. Mengel, E. R. Talaat, H. S. Porter, and K. L. Chan, 2003: Planetary-scale inertio gravity waves in the mesosphere. *Geophys. Res. Lett.*, **30**, 2228, https://doi.org/10.1029/2003GL018376.

——, ——, ——, ——, and ——, 2004: Properties of internal planetary-scale inertio gravity waves in the mesosphere. *Ann. Geophys.*, **22**, 3421–3435, https://doi.org/10.5194/angeo-22-3421-2004.

McKee, T., N. Doesken, and J. Kleist, 1993: The relationship of drought frequency and duration to time scales. *Proc. Eighth Conf. on Applied Climatology*, Anaheim, CA, Amer. Meteor. Soc., 179–183.

Mekonnen, A., and C. D. Thorncroft, 2016: On mechanisms that determine synoptic time scale convection over East Africa. *Int. J. Climatol.*, **36**, 4045–4057, https://doi.org/10.1002/joc.4614.

——, ——, and A. R. Aiyyer, 2006: Analysis of convection and its association with African easterly waves. *J. Climate*, **19**, 5405–5421, https://doi.org/10.1175/JCLI3920.1.

——, ——, ——, and G. N. Kiladis, 2008: Convectively coupled Kelvin waves over tropical Africa during the boreal summer: Structure and variability. *J. Climate*, **21**, 6649–6667, https://doi.org/10.1175/2008JCLI2008.1.

Mounier, F., G. N. Kiladis, and S. Janicot, 2007: Analysis of the dominant mode of convectively coupled Kelvin waves in the West African monsoon. *J. Climate*, **20**, 1487–1503, https://doi.org/10.1175/JCLI4059.1.

——, S. Janicot, and G. N. Kiladis, 2008: The West African monsoon dynamics. Part III: The quasi-biweekly zonal dipole. *J. Climate*, **21**, 1911–1928, https://doi.org/10.1175/2007JCLI1706.1.

Mozer, J. B., and J. A. Zehnder, 1996: Lee vorticity production by large-scale tropical mountain ranges. Part II: A mechanism for the production of African waves. *J. Atmos. Sci.*, **53**, 539–549, https://doi.org/10.1175/1520-0469(1996)053<0539:LVPBLS>2.0.CO;2.

NGDC, 1988: 5-minute Gridded Global Relief Data (ETOPO5). National Geophysical Data Center, accessed 2 October 2017, https://doi.org/10.7289/V5D798BF.

Nguyen, H., and J.-P. Duvel, 2008: Synoptic wave perturbations and convective systems over equatorial Africa. *J. Climate*, **21**, 6372–6388, https://doi.org/10.1175/2008JCLI2409.1.

Peatman, S. C., A. J. Matthews, and D. P. Stevens, 2014: Propagation of the Madden–Julian oscillation through the Maritime Continent and scale interaction with the diurnal cycle of precipitation. *Quart. J. Roy. Meteor. Soc.*, **140**, 814–825, https://doi.org/10.1002/qj.2161.

Pohl, B., S. Janicot, B. Fontaine, and R. Marteau, 2009: Implication of the Madden–Julian oscillation in the 40-day variability of the West African monsoon. *J. Climate*, **22**, 3769–3785, https://doi.org/10.1175/2009JCLI2805.1.

Reed, R. J., D. C. Norquist, and E. E. Recker, 1977: The structure and properties of African wave disturbances as observed during phase III of GATE. *Mon. Wea. Rev.*, **105**, 317–333, https://doi.org/10.1175/1520-0493(1977)105<0317:TSAPOA>2.0.CO;2.

Riehl, H., 1945: Waves in the easterlies and the polar front in the tropics. University of Chicago Misc. Rep. 17, 79 pp.

Riley, E. M., B. E. Mapes, and S. N. Tulich, 2011: Clouds associated with the Madden–Julian oscillation: A new perspective from *CloudSat*. *J. Atmos. Sci.*, **68**, 3032–3051, https://doi.org/10.1175/JAS-D-11-030.1.

Roehrig, R., F. Chauvin, and J.-P. Lafore, 2011: 10–25-day intraseasonal variability of convection over the Sahel: A role of the Saharan heat low and midlatitudes. *J. Climate*, **24**, 5863–5878, https://doi.org/10.1175/2011JCLI3960.1.

Roundy, P. E., 2018: A wave-number frequency wavelet analysis of convectively coupled equatorial waves and the MJO over the Indian Ocean. *Quart. J. Roy. Meteor. Soc.*, **144**, 333–343, https://doi.org/10.1002/qj.3207.

——, and W. M. Frank, 2004: A climatology of waves in the equatorial region. *J. Atmos. Sci.*, **61**, 2105–2132, https://doi.org/10.1175/1520-0469(2004)061<2105:ACOWIT>2.0.CO;2.

——, and M. A. Janiga, 2012: Analysis of vertically propagating convectively coupled equatorial waves using observations and a non-hydrostatic Boussinesq model on the equatorial beta-plane. *Quart. J. Roy. Meteor. Soc.*, **138**, 1004–1017, https://doi.org/10.1002/qj.983.

Sakaeda, N., G. Kiladis, and J. Dias, 2017: The diurnal cycle of tropical cloudiness and rainfall associated with the Madden–Julian oscillation. *J. Climate*, **30**, 3999–4020, https://doi.org/10.1175/JCLI-D-16-0788.1.

Schreck, C. J., L. Shi, J. P. Kossin, and J. J. Bates, 2013: Identifying the MJO, equatorial waves, and their impacts using 32 years of HIRS upper-tropospheric water vapor. *J. Climate*, **26**, 1418–1431, https://doi.org/10.1175/JCLI-D-12-00034.1.

Sinclaire, Z., A. Lenouo, C. Tchawoua, and S. Janicot, 2015: Synoptic Kelvin type perturbation waves over Congo basin over the period 1979–2010. *J. Atmos. Sol. Terr. Phys.*, **130–131**, 43–56, https://doi.org/10.1016/j.jastp.2015.04.015.

Skinner, C. B., and N. S. Diffenbaugh, 2013: The contribution of African easterly waves to monsoon precipitation in the CMIP3

ensemble. *J. Geophys. Res. Atmos.*, **118**, 3590–3609, https://doi.org/10.1002/jgrd.50363.

Sultan, B., and S. Janicot, 2003: The West African monsoon dynamics. Part II: The "preonset" and "onset" of the summer monsoon. *J. Climate*, **16**, 3407–3427, https://doi.org/10.1175/1520-0442(2003)016<3407:TWAMDP>2.0.CO;2.

——, ——, and A. Diedhiou, 2003: The West African monsoon dynamics. Part I: Documentation of intraseasonal variability. *J. Climate*, **16**, 3389–3406, https://doi.org/10.1175/1520-0442(2003)016<3389:TWAMDP>2.0.CO;2.

——, C. Baron, M. Dingkuhn, B. Sarr, and S. Janicot, 2005: Agricultural impacts of large-scale variability of the West African monsoon. *Agric. For. Meteor.*, **128**, 93–110, https://doi.org/10.1016/j.agrformet.2004.08.005.

Takayabu, Y. N., and T. Nitta, 1993: 3–5 day-period disturbances coupled with convection over the tropical Pacific Ocean. *J. Meteor. Soc. Japan*, **71**, 221–246, https://doi.org/10.2151/jmsj1965.71.2_221.

Tan, H., P. Ray, B. S. Barrett, M. Tewari, and M. W. Moncrieff, 2018: Role of topography on the MJO in the maritime continent: A numerical case study. *Climate Dyn.*, https://doi.org/10.1007/s00382-018-4275-3.

Taubenheim, J., 1974: Zur Berücksichtigung der Autokorrelation bei der statistischen Signifikanzprüfung von Korrelation zwischen zwei Zeitreihen. *Gerlands Beitr. Geophys.*, **83**, 121–128.

Thiawa, W. M., S. Janicot, K. H. Cook, B. Fontaine, A. Mekonnen, O. Ndiaye, P.-H. K. Tamo, and E. K. Vizy, 2017: Subseasonal forecasting. *Meteorology of Tropical West Africa: The Forecasters' Handbook*, D. J. Parker and M. Diop-Kane, Eds., John Wiley & Sons, 255–288.

Thorncroft, C. D., and B. J. Hoskins, 1994: An idealized study of African easterly waves. I: A linear view. *Quart. J. Roy. Meteor. Soc.*, **120**, 953–982, https://doi.org/10.1002/qj.49712051809.

——, N. M. J. Hall, and G. N. Kiladis, 2008: Three-dimensional structure and dynamics of African easterly waves. Part III: Genesis. *J. Atmos. Sci.*, **65**, 3596–3607, https://doi.org/10.1175/2008JAS2575.1.

——, H. Nguyen, C. Zhang, and P. Peyrillé, 2011: Annual cycle of the West African monsoon: Regional circulations and associated water vapour transport. *Quart. J. Roy. Meteor. Soc.*, **137**, 129–147, https://doi.org/10.1002/qj.728.

Tindall, J. C., J. Thuburn, and E. J. Highwood, 2006a: Equatorial waves in the lower stratosphere. I: A novel detection method. *Quart. J. Roy. Meteor. Soc.*, **132**, 177–194, https://doi.org/10.1256/qj.04.152.

——, ——, and ——, 2006b: Equatorial waves in the lower stratosphere. II: Annual and interannual variability. *Quart. J. Roy. Meteor. Soc.*, **132**, 195–212, https://doi.org/10.1256/qj.04.153.

Tseng, W.-L., H.-H. Hsu, N. Keenlyside, C.-W. J. Chang, B.-J. Tsuang, C.-Y. Tu, and L.-C. Jiang, 2017: Effects of surface orography and land–sea contrast on the Madden–Julian oscillation in the Maritime Continent: A numerical study using ECHAM5-SIT. *J. Climate*, **30**, 9725–9741, https://doi.org/10.1175/JCLI-D-17-0051.1.

Tulich, S. N., and G. N. Kiladis, 2012: Squall lines and convectively coupled gravity waves in the tropics: Why do most cloud systems propagate westward? *J. Atmos. Sci.*, **69**, 2995–3012, https://doi.org/10.1175/JAS-D-11-0297.1.

van der Linden, R., A. H. Fink, J. G. Pinto, T. Phan-Van, and G. N. Kiladis, 2016: Modulation of daily rainfall in southern Vietnam by the Madden–Julian oscillation and convectively coupled equatorial waves. *J. Climate*, **29**, 5801–5820, https://doi.org/10.1175/JCLI-D-15-0911.1.

Ventrice, M. J., and C. D. Thorncroft, 2013: The role of convectively coupled atmospheric Kelvin waves on African easterly wave activity. *Mon. Wea. Rev.*, **141**, 1910–1924, https://doi.org/10.1175/MWR-D-12-00147.1.

——, ——, and P. E. Roundy, 2011: The Madden–Julian oscillation's influence on African easterly waves and downstream tropical cyclogenesis. *Mon. Wea. Rev.*, **139**, 2704–2722, https://doi.org/10.1175/MWR-D-10-05028.1.

Vogel, P., P. Knippertz, A. H. Fink, A. Schlueter, and T. Gneiting, 2018: Skill of global raw and postprocessed ensemble predictions of rainfall over northern tropical Africa. *Wea. Forecasting*, **33**, 369–388, https://doi.org/10.1175/WAF-D-17-0127.1.

Wheeler, M., and G. N. Kiladis, 1999: Convectively coupled equatorial waves: Analysis of clouds and temperature in the wavenumber–frequency domain. *J. Atmos. Sci.*, **56**, 374–399, https://doi.org/10.1175/1520-0469(1999)056<0374:CCEWAO>2.0.CO;2.

——, and H. H. Hendon, 2004: An all-season real-time multivariate MJO index: Development of an index for monitoring and prediction. *Mon. Wea. Rev.*, **132**, 1917–1932, https://doi.org/10.1175/1520-0493(2004)132<1917:AARMMI>2.0.CO;2.

Yang, G.-Y., B. Hoskins, and J. Slingo, 2003: Convectively coupled equatorial waves: A new methodology for identifying wave structures in observational data. *J. Atmos. Sci.*, **60**, 1637–1654, https://doi.org/10.1175/1520-0469(2003)060<1637:CCEWAN>2.0.CO;2.

——, ——, and ——, 2007: Convectively coupled equatorial waves. Part I: Horizontal and vertical structures. *J. Atmos. Sci.*, **64**, 3406–3423, https://doi.org/10.1175/JAS4017.1.

Yasunaga, K., and B. Mapes, 2012: Differences between more divergent and more rotational types of convectively coupled equatorial waves. Part II: Composite analysis based on space–time filtering. *J. Atmos. Sci.*, **69**, 17–34, https://doi.org/10.1175/JAS-D-11-034.1.

Zhou, X., and B. Wang, 2007: Transition from an eastern Pacific upper-level mixed Rossby–gravity wave to a western Pacific tropical cyclone. *Geophys. Res. Lett.*, **34**, L24801, https://doi.org/10.1029/2007GL031831.